

TECHNICAL UNIVERSITY OF CIVIL ENGINEERING

Faculty of Building Services

Department of Thermo-Hydraulic Systems and Atmospheric Protection

RESEARCH REPORT 3

NUMERICAL STUDY ON THE CONDENSATION
PHENOMENON IN VEHICLES IN ORDER TO IMPROVE THE
EFFICIENCY OF THE DEMISING SYSTEMS

Coordinator

Associate prof. Ph.D. Cătălin TEODOSIU

Ph.D. Student

Alexandra ANGELESCU (ENE)

BUCHAREST 2022

Table of content

1.	Introduction	5
2.	Condensation phenomenon	. 11
	2.1. Types of condensation	. 11
	2.2. CFD techniques to assess the condensation phenomenon	. 13
	2.2.1. Multiphase models	. 14
	2.2.2. Single phase models	.16
3.	Description of the numerical study	. 23
	3.1. Geometry generation	. 23
	3.2. Mesh generation	. 24
	3.3. Numerical model	. 25
	3.4. Radiation heat transfer	. 25
	3.5. Condensation process	. 25
	3.6. Boundary conditions	. 26
3.	7. Studied cases	. 27
4.	Results	. 29
5.	Conclusions	.46
6.	Perspectives	. 47
R	eferences	.48

List of figures

Fig. 1 – Types of heating systems in EV [13]	7
Fig. 2 – schematic diagram of the AC / heat pump / dual heat pump in vehicles [18]	9
Fig. 3 – temperature of 20 °C reached for the three analysed cases [20]	10
Fig. 4 – schematic figure of filmwise and dropwise condensation	
(https://www.semanticscholar.org/paper/Direct-and-Indirect-Contact-Filmwise-as-well-as-of-	
Bhuyan/569e16b61a5fda236e85d9bb2c4ce014e7a7593a)	12
Fig. 5 – The phase diagram [28]	
Fig. 6 – Exemplification of the mesh geometry near the wall	21
Fig. 7 – The experimental stand during different stages in its construction	24
Fig. 8 – Mesh display	24
Fig. 9 – Description of the moving source term from one centre of the cell to the one next to it [36].	26
Fig. 10 – Variation of supply air temperature in time within the vehicle [37]	27
Fig. 11 – Supply air temperature variation in time	28
Fig. 12 – Mass flow rate of water vapours condensation for cases with the same air supply	
temperature	29
Fig. 13 - Mass flow rate of water vapours condensation for cases with variation of air supply	
temperature depending on the velocity	30
Fig. 14 – Comparison of mass flow rate of water vapours condensation for 9 m/s air supply at	
different thermal power of the heating system	30
Fig. 15 – Comparison of mass flow rate of water vapours condensation for 6 m/s air supply at	
different thermal power of the heating system	31
Fig. 16 – Comparison of mass flow rate of water vapours condensation for 3 m/s air supply at	
different thermal power of the heating system	
Fig. 17 – Mass flow rate of water vapours condensation windshield contour at 5 seconds	
Fig. 18 – Mass flow rate of water vapours condensation windshield contour at 20 seconds	
Fig. 19 – Mass flow rate of water vapours condensation windshield contour at 40 seconds	
Fig. 20 – Mass flow rate of water vapours condensation windshield contour at 60 seconds	
Fig. 21 – Mass flow rate of water vapours condensation windshield contour at 80 seconds	
Fig. 22 – Mass flow rate of water vapours condensation windshield contour at 100 seconds	
Fig. 23 – Temperature contour on the windshield at 5 seconds	
Fig. 24 – Temperature contour on the windshield at 20 seconds	
Fig. 25 – Temperature contour on the windshield at 40 seconds	
Fig. 26 – Temperature contour on the windshield at 60 seconds	45

1. Introduction

The world is more and more concerned about the energy consumption in buildings, transportation, industry and processes. On one hand this concern is related to the pollution levels that have been raising constantly in the last few decades becoming a real threat for the future of humankind. On the other hand, the natural resources are more and more difficult to be extracted leading to an increased concern in the future possibilities to produce and store energy. Therefore, the population started to feel the impact and importance of the energy consumption worldwide, especially through the lens of education, sustainability and most recently, through the invoice prices that to not seize to go down.

As the cities around the globe are getting bigger and bigger every day, the transportation field is increasing as a result of this process. People present the need for mobility which leads to an increase in the pollution segments as a result. The electric vehicles came with a solution in this direction. Whilst the internal combustion engine (ICE) emits gases such as CO_2 and NO_x which can be very dangerous for the body, the fuel cells electric vehicles (FC) came as a response to this issue by using the hydrogen as the main transportation fuel, which only release water [1].

The statistics show that the recent events did have an impact on the energy consumption in transportation sector. The restriction mobility during the pandemic period reduced the energy necessity (in 2020) by 13 % compared to the rates in 2019. This represented a huge achievement given the increasing trend that was constantly felt in the last seven years in transportation field [2]. Moreover, in 2020 the energy consumption remained the same of the households, but dropped by 5.6 % in commercial and public buildings [2]. These results were also linked to the lockdown periods when people did not have access to these sorts of services.

According the Eurostat [3], the European economy is based on oil and petrol, while the natural gas kept its second place. Nonetheless, 2020 came with a decrease in their usage by 12.6% for oil and 2.4% in gas [3]. This decrease was considered based on the pandemic period on one hand, but also due to the increase in renewable energy contribution which continues to grow. The same statistics showed that renewable energies gained terrain in front of the solid fossil fuels starting 2018 [3]. Moreover, the solid fuels usage decreased by 18.4% in 2020 reaching the lowest value since 1990 [3].

Transportation emissions are primary comprised of CO₂, CH₄ and NO₂. Nonetheless, at a global level, the CO₂ emissions are responsible for 95% of the transportation greenhouse gas emissions [4]. As the need to respond to the global warming threat, solving the greenhouse gas emissions from the transportation field is highly important. Nowadays, electric vehicles seem to represent the response to this issue. However, electric vehicles were developed even from the early days of the industrial revolution. At that time, the competition between the EV and the ICEV established the winner in four stages such as, the formative years of the automobile industry (1885 – 1905), imposing the oil as a dominant option in car industry (1905 – 1920), followed by a consolidation of the ICEV between 1920 – 1973 and further led to a questioning of the oil consumption impact (1973 – 1998) [4]. After 1998, the escape from the

ICEV dominant market has started through the development of the EV manufacturers. Nonetheless, at the moment the EVs still show a lower life cost per km in comparison to the ICEV and still need more improvement. In addition, some of the challenges to adapt the EVs at the expense of the ICEV are represented by the acquisition and range prices of EVs. The factors are interconnected as increasing the battery pack can solve the issue of driving range, but at the same time will raise the design complexity of the car by improving the necessary cooling systems, and will also increase the vehicles' cost [4]. Therefore, a fine balance between the driving range, the technology and prices should be found.

The European Green Deal was presented at the beginning of the pandemic period as a response to the constant increase in the energy consumption and pollution levels. Furthermore, in July 2021 a new program named "Fit for 55" was launched by the European Commission in order to push the legislation towards a more sustainable future. This new program "Fit for 55" challenges directly the oil consumption and road transportation, proposing a new emission trading system for buildings and the development of alternative fuels infrastructure, and banning the usage of internal combustion engine cars by 2035 [5]. Some countries such as Sweden, went ahead of the European legislation choosing to set a decrease in the emissions from the personal transportation by at least 70 % by 2030 and introduced a policy that bans the ICEV usage by 2030 instead of 2035 [6].

Given this concern towards the energy consumption, especially the usage of fossil fuels in transportation, the hybrid vehicles and full electric vehicles have been starting to gain ground on the market. People are choosing more and more this alternative means of transportation that becomes more and more popular [7]. More than 1 million electric vehicles were sold in 2017, a number that increased with 54% than in 2016 [8]. 5.1 million EV were sold globally in 2018, which was almost double in comparison to 2017 [9]. In 2018, Norway recorded the highest number of electric vehicles market, more exactly 39.2%, Iceland 11.7% and Sweden 6.3%, China 2.2%, Germany 1.6%, USA 1.2% and Japan 1.0% [8]. In 2019, 7 992 535 electric vehicles were registered worldwide [8]. In 2020, the statistics showed that the EV sales exceeded 10 million globally and it is projected to reach 230 million EV by 2023 [6]. However, the electric vehicles not only present insufficient waste energy to warm up the interior cabin, but they are also highly influenced by the heating system usage which can significantly reduce the power train and the driving range.

The necessity of a heating system inside the passenger compartment of a vehicle goes in two directions, the first one is related to the defogging and de-icing of the glazing surfaces with highly important impact on the visibility and safety driving experience, and a second one related to comfort conditions for the occupants including air velocity, temperature and humidity levels. Whilst both seem important, the electrical vehicles, including the full electrical vehicles (EV) and the hybrid electric vehicles (HEV) present huge deficiencies in this regard. In winter conditions the internal combustion engine can benefit from a waste energy for heating purposes of around 5 kW, whilst the electric vehicles can gather only around 2 kW at a temperature of around 40 °C which is highly insufficient to maintain the interior comfort conditions and the visibility safety conditions [10, 11]. This will eventually lead to a usage of the batteries which will further reduce the power train and the driving range [11].

The air conditioning (AC) unit represents the system that provides cooling, heating and ventilation when it comes to electric vehicles. This includes all types of electrical vehicles such

as full electric vehicles, hybrid vehicles and fuel cell electric vehicles. The AC unit helps control the interior parameters, such as temperature, velocity and humidity levels, inside the passenger compartment providing the safety driving needs. At the same time the EV present also a thermal management of the battery pack which is highly important in order to prevent premature aging and loss capacity of these systems. Therefore, the thermal management and the AC units have to work together in order to provide the proper interior conditions. As the AC represents the most energy consumption from the auxiliary systems causing in general a decrease in driving range of 30-40 % depending on the type of vehicle and the volume [12].

The HVAC systems for electric vehicles are composed of an air conditioning system, an electric water heater (PTC) and a heat exchanger that generates cold water for battery cooling system. The electric heater power of a normal personal vehicle is 5.5 kW and the air conditioning is 3.5 kW [13]. Depending on the COP values the electric power varies between 1.5 - 5 kW. 2 kW of electric water heater power is used for heating the battery and 3.5 kW for passenger compartment heating necessities [13]. Moreover, for demisting and defrosting the glazing surfaces, the European regulations [14] require to use the maximum levels of power, leading to an electric energy of 7 - 7.5 kW under 0 °C. Therefore, the electric vehicles require a very efficient systems in order to minimize the impact on the autonomy of the car [13].

The heating methods present in electric vehicles are the following ones [13]:

- Electric heater: this is the most common equipment used in EVs, is purely dissipative and requires very simple installation. Its efficiency: <1.
- Fuel burner: this system requires a fuel tank. Its efficiency: <1.
- Hot gas: requires an adaptation of the AC system. Its efficiency: <1.
- Heat pump: this system is more efficient than the PTC heater. Its efficiency: >2 [13].

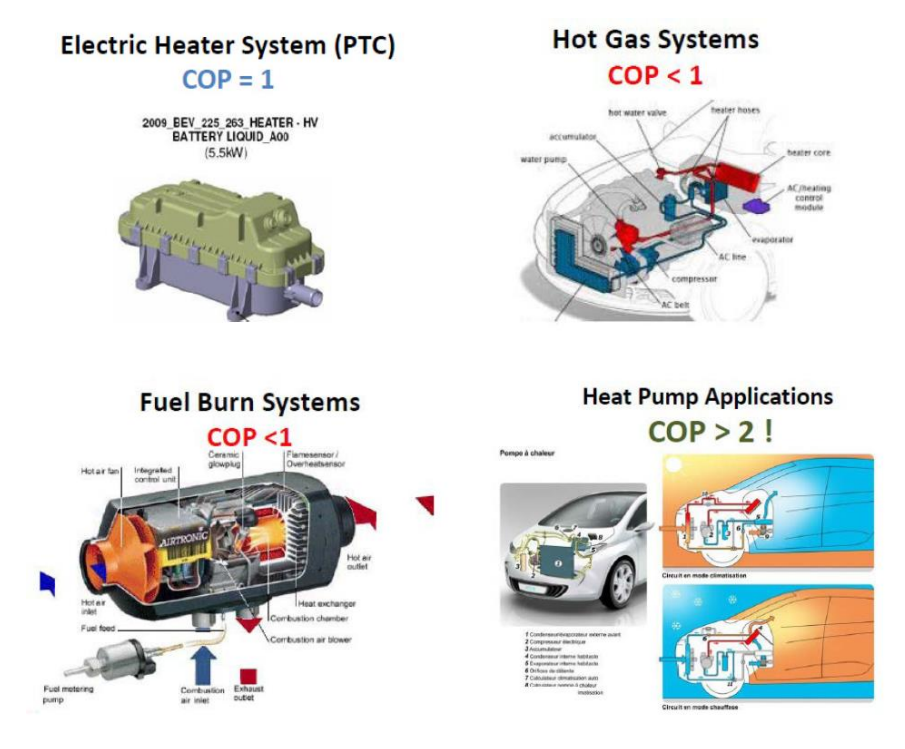


Fig. 1 – Types of heating systems in EV [13]

The usage of heat pumps in electric vehicles can help to save up to 50% of the energy needed to warm up the interior passenger cabin. For cold regions, depending on the driving cycle, the driving range on an electrical vehicle can be extended from 10-30% due the heating system usage [8].

The vehicle can be cooled and heated by means of thermoelectric modules. These modules present a huge advantage as they do not include any moving parts, meaning that the sound pressure levels are not influenced by their use. Moreover, this equipment is small, has a long lifetime period, as it does not contain moving parts and can produce a very good temperature control. Nonetheless, this technology could not be accepted in the industry due to its very poor efficiency. However, the modules are indeed used for heating and colling certain parts of vehicles, especially in the luxury vehicles' industry such as for seat and steering wheel heating/cooling [15].

The usage of a PTC heater could provide the necessary heat to suppress the heat losses, but as its energy is provided by the battery system, the results showed a drop of 24% in the driving range of a fully electrical vehicle [15]. Another study found that the heat pump usage instead of PTC heaters in EV for heating mode could lead as much as 17-52% energy saving depending on the climate and region [16]. For instance, for the Italian region, the energy need to maintain the comfort conditions while using an EV is found between 200-250 kWh, meaning around 10-13% of the traction energy power [16]. Furthermore, the AC usage showed a reduction in driving range from 94 km to 68 km [16]. In another set of challenges, a heating device for EV using ethanol was compared with a full electric heater and the results showed that the electric heater would reduce the driving range by 12.02 kWh, meaning a reduction by 30% of the driving range [17]. On the other hand, the ethanol heating system would have taken only 3.17 kWh from the battery system [17].

Other studies found that using the AC or the heater, more exactly the i-MiEV system developed by Mitsubishi Motors Corporation leads to a reduction of the driving range between 15-45% [12].

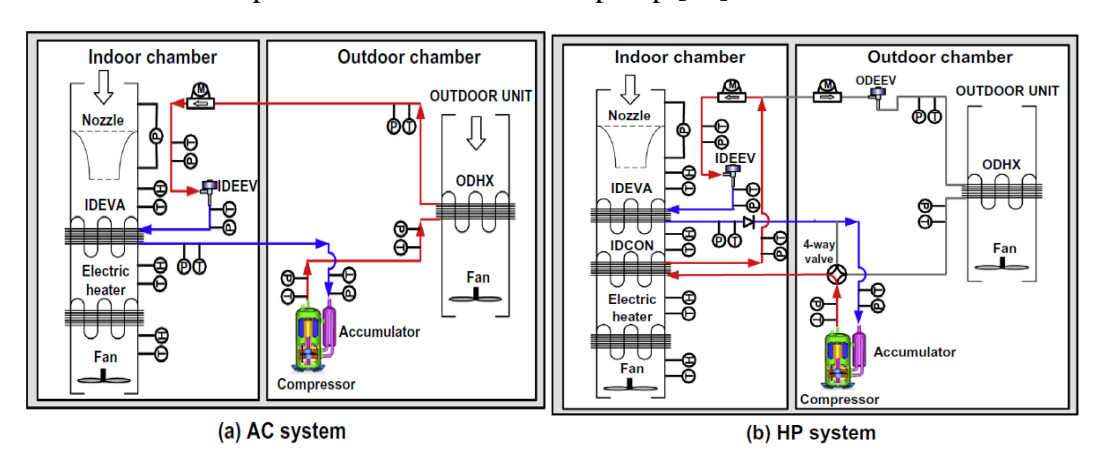
As the fogging process can hinder driving safety, providing a comfortable and safe environment is highly necessary. In colder regions, heating up the interior cabin together with the dehumidifying process is necessary in order to help the demisting process to take place. Using an AC unit for the cabin vehicles helps to reduce this process [18]. The issue is that the sensible air cooling in the dehumidifying process decreases the air temperature that further is introduced in the heater, leading to an increase in power consumption. As a response to this issue, heat pumps were introduced into the equation [18]. The heat pumps contain a compressor, an outdoor heat exchanger, an indoor evaporator, an expansion valve and in comparison with the AC unit contains also an indoor condenser and a 4-way valve [18]. For colder periods the indoor condenser and the outdoor heat exchanger work as a condenser and as an evaporator. During the periods when the dehumidifying process is needed, the interior air is cooled, meaning dehumidified in the indoor evaporator [18]. The air is further heated by means of the indoor condenser and in some cases with an electric heater, if needed [18]. Furthermore, it was observed that an additional waste heat recovery operation can be developed. This idea led to a new system named dual heat pump [18].

As shown in the figures below the process in the heat pump system starts at the condensed liquid in the IDCON which further goes into the IDEVA through IDEEV. The thermal agent which was evaporated in the IDEVA component reaches the compressor. The

indoor air is cooled and dehumidified the IDEVA component and further heated in IDCON and electric heater before being introduced at the interior of the vehicle [18].

In the second type of system, meaning the dual heat pump, the process is a bit different. The thermal agent in liquid form in IDCON splits into ODHX and IDEVA. The ODHX helps to gain some heat from the outdoor air, and IDEVA helps to do the same from the indoor air. The indoor air is cooled and dehumidified at IDEVA level and then heated at IDCON and electric heater if further needed [18].

A comparison between the three systems showed that the COP raised by 180% for the heat pump in comparison with the AC unit at the indoor wet bulb temperature of 15 °C. Furthermore, for an indoor wet bulb temperature of 13 °C, the COP of the dual heat pump raised with 62% in comparison to the normal heat pump [18].



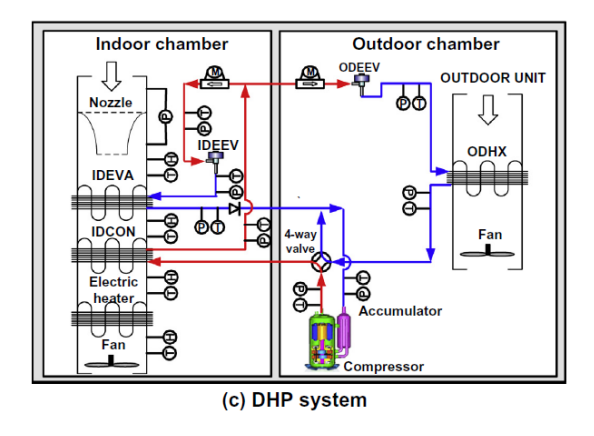


Fig. 2 – schematic diagram of the AC / heat pump / dual heat pump in vehicles [18]

Another way in approaching this issue proposed a novel high efficiency HVAC system which provides the conventional AC unit together with a Pure Heat Pump and also a Defog Heat Pump [19]. This new system consisting mainly in the defogging heat pump represents a combination of two heat exchangers, meaning an evaporator and a condenser, and a heater. The performance of all these three systems together was evaluated experimentally at the lab scale [19]. The results showed that when using the defog heat pump the interior air at 27 °C was dehumidified, and the temperature dropped to 17 °C by the evaporator. It then went through the condenser where it received heat up to a temperature of 40 °C [19]. In AC mode only, the

temperature inside the cabin drops from 25 °C to 15 °C in five minutes. In heat pump mode only, the study showed a rise in temperature from 30 °C to 40 °C in 10 minutes of use [19].

The impact of the HVAC systems on the demisting/defrost process was compared in a study comprising three different vehicles an internal combustion engine, an electric vehicle using an electrical resistance and an electrical vehicle using a heat pump [20].

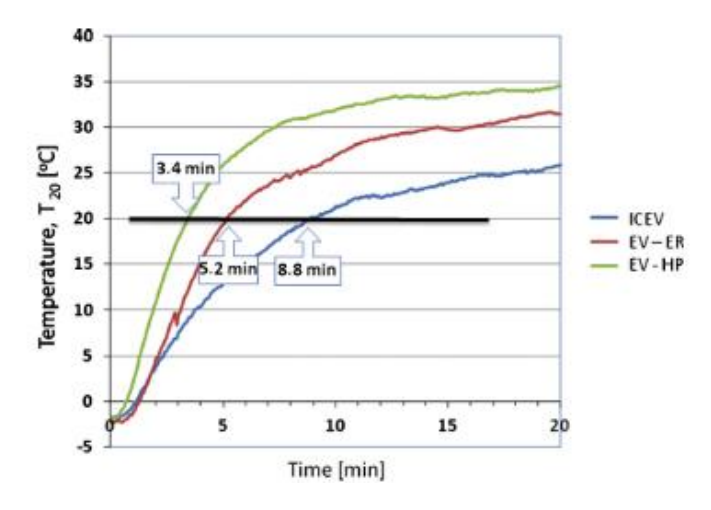


Fig. 3 – temperature of 20 °C reached for the three analysed cases [20]

The studies were conducted by using infrared camera (IR) for determining the windshield temperature on three windshields showed that the electrical vehicles using heat pumps (blue line) needed 3.4 min, the electrical vehicles using electrical resistance needed 5.2 minutes (red line), while the internal combustion engine needed almost 9 minutes to reach a temperature of 20 °C at the windshield. This technique proved that IR technology can be a useful tool to determine the temperatures at the windshield level. However, these measurements need to be treated with care and attention due to high levels of errors that can occur due to faults in predicting the emissivity factor [20].

Improving the demisting system in vehicles might not be as easy as it seems. This process is complex due to the actual flow at the defrosting/demisting exit. The reason behind some of these complexities are related to the air jets which usually are rectangular, they are positioned in an obliquely impinging angle which generates turbulence and non-uniformities in these already complex geometries [21]. A study by Nasr et. al. [21] showed through an experimental approach that the velocity profiles at the air supply are quite non-uniform which leads to a non-symmetric and non-uniform temperature distribution on the inner surface of the windshield [21].

This finding is supported by another experimental approach which was conducted in a climatic chamber on two different electric vehicles, a small vehicle and a large one [8]. The results on both vehicles showed that the heating system produced a "stronger" effect on the driver' side compared to the other areas [8]. This phenomenon was interpreted as an intentional comfort condition imposed by the manufacturer by setting a portion of air injection in the direction of the driver [8]. Moreover, the vehicle presenting a smaller heat pump and an engine power encountered significant issues in achieving the interior temperature when confronted with negative ambient temperature [8].

Furthermore, an approach to lower the fogging process on the windshield of a vehicle was proposed as a combination of maximum-return-air in order to reduce de heating demand [22]. This was done for winter period with temperatures found between - 5 °C and - 20 °C and was implemented through a curtain of air imposed on the windshield. The results proved that the heating necessities could be decreased by 46.4 - 62.1 % compared to an all-fresh-air condition [22].

Another study based on the subject of heat pumps in electric vehicles conducted through an experimental approach showed that, using a heat pump system is insufficient to replace the conventional PTC heater for an exterior temperature of -10 °C, meaning that at this outdoor temperature a small capacity of the electric heater must be used together with the heat pump system in order to save energy and provide the thermal comfort for the passengers [23]. Nonetheless, generally the usage of the heat pump should be necessary for thermal comfort and safe driving conditions [23].

2. Condensation phenomenon

2.1. Types of condensation

When the temperature difference between the solid surface and the interior air is sufficiently large, the fluid or the surface may experience a change of phase. The condensation phenomenon has been a front topic in buildings for many reasons, such as energy consumption, comfort conditions and health issues. The appearance of condensation phenomenon inside buildings takes place generally on the walls and glazing surfaces due to a drop in the temperature in the region correlated with the high level of water vapours. If the temperature of the solid surfaces drops below the dew point temperature, the condensation phenomenon takes place. This leads to a release of heat in the area together with a drop in the water vapours content.

The condensation phenomenon can take place directly in the bulk of the fluid and this phenomenon can be called direct-contact condensation, or it can take place on a solid surface, and this is called surface condensation.

The surface condensation phenomenon can take the following forms:

- filmwise condensation
- dropwise condensation

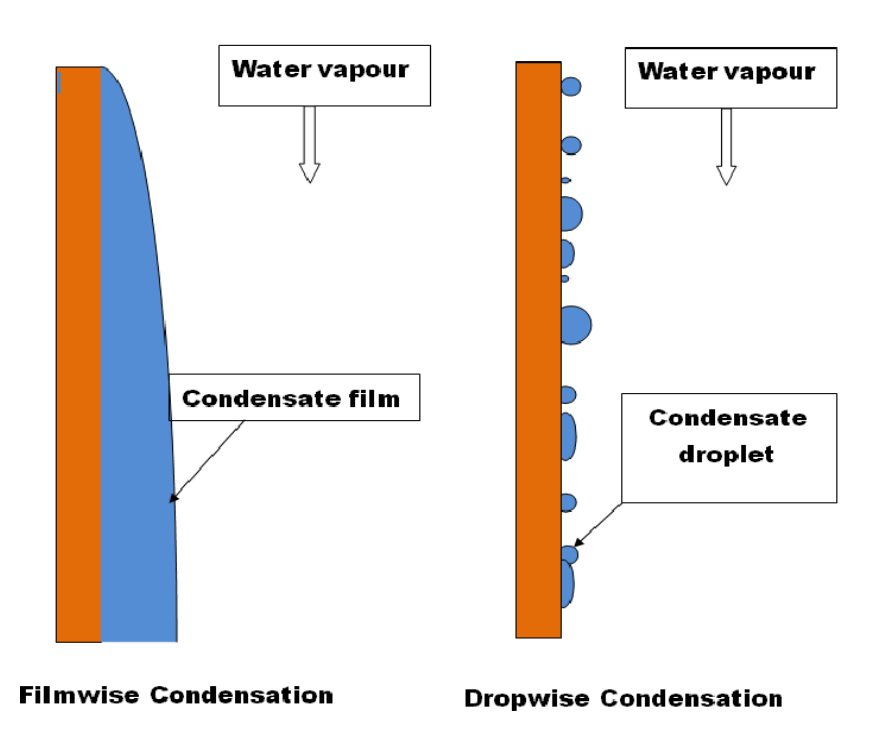


Fig. 4 – schematic figure of filmwise and dropwise condensation (https://www.semanticscholar.org/paper/Direct-and-Indirect-Contact-Filmwise-as-well-as-of-Bhuyan/569e16b61a5fda236e85d9bb2c4ce014e7a7593a)

A continuous thin film condensation takes place on a surface when the surface tension between the liquid and the solid material is generally very small. This sort of condensation needs to present a surface that is clean, non-greasy, smooth and free of any scratches, practically free of any materials that can become nucleation sites. This type of condensation is generally associated with the steam condensation on a clean metal surface.

For a surface tension that is large, the condensation coalescence into a large number of droplets of different sizes. The droplets grow as the condensation phenomenon continues to take place. The condensation phenomenon in this case in generated by a point on the solid surface where an imperfection is present, such as dust particles, scratches etc. These imperfections are called nucleation sites.

According to the literature, the heat transfer coefficient when dropwise condensation takes place is approximately 10 times higher than the heat transfer coefficient when filmwise condensation is in place. Therefore, in engineering applications such as condensers design, it is recommended to have a dropwise condensation instead of a filmwise [24]. Therefore, in order to promote this type of condensation, the following actions can be implemented [24]:

- coating the condensation surface with a special substance such as oil, wax, kerosene, oleic acid etc.
- injecting non-wetting chemicals into the water vapours.
- Coating the solid surface with a polymer with low surface energy, such as teflon, silicon, gold, silver etc.

The first two mentioned methods are time dependent as after a while they won't be able to contain the coating materials. When it comes to external coatings such as Teflon, this method

can slower the condensation phenomenon as it has a low thermal conductivity [24]. Therefore, a coating thicker than 20 µm leads to a raise in the conduction resistance higher than the heat transfer augmentation effect due to dropwise condensation generation [24].

Dropwise condensation is a complicated phenomenon to analyse due to several factors such as intermittent time-dependent character, the surface tension and its dominance over the entire phenomenon, meaning the size and the shape of the droplets, the position and the presence of the nucleation sites, as well as the time when the droplets would start their movement towards to lower part of the surface [24].

Both types of condensation are found in practice, and they can even occur simultaneously [25]. However, the filmwise condensation is predominant in engineering applications, in electronic devices, construction materials, air conditioning systems and on glazing surfaces [25]. Moreover, when the condensation phenomenon occurs, the energy transfer increases as the water condensed on the solid surface massively reduced the thermal insulation of the solid surface material. It seems the condensation film leads to an increase in the convective heat transfer coefficient between the solid surface and the interior air [25].

2.2. CFD techniques to assess the condensation phenomenon

The condensation phenomenon can be assessed through an experimental or a numerical assessment. Due to the fact that the present paper will evaluate the surface condensation phenomenon through a numerical approach using the CFD models, the next pages will cover this subject.

The CFD technique is the only method that can take into account the integration of all phenomena that are influencing the condensation process, such as, mass conservation, energy conservation and momentum conservation. Furthermore, the CFD technique can determine the exact location and evolution in space and time of the condensation process.

The condensation phenomenon can be treated in a wide range of evaluations in CFD models. For instance, a simple analysis using the CFD method applies a simple comparison between the dew point temperature of the ambient air and temperature of the solid surface in order to determine if and when the condensation process would start [26, 27]. Even the novel studies in the literature [28] chose to use this method as this approach is simple and effective. Nonetheless, such methods are rudimentary as they do not take into consideration the real condensation phenomenon with all the other parameters that influence its appearance and development such as sensible heat due to vaporisation, latent heat release due to condensation and influence of the mass and energy transfers. Furthermore, such simple evaluations of the condensation phenomenon do not provide important information as the quantity on the condensed water vapours. However, they do provide the location and evolution in time.

Other complex CFD models can assess the condensation phenomenon through two main methods: monophase and multiphase concepts.

The multiphase method imposes the fluid as a mixture of water vapours and air and another phase of water liquid. Therefore, two sets of equations are needed in order to evaluate the condensation phenomenon. Furthermore, as there is an interaction between the two phases,

there is a need to introduce new source terms which will evaluate these interactions in the conservation equations.

The monophase concept oversees the condensation phenomenon through a mixture species of water vapours and air. This method requires only one set of equations as there is only one phase.

2.2.1. Multiphase models

The most common multiphase model used in Ansys Fluent is also known as the Lee model. When the Eulerian multiphase model is used in conjunction with the two-resistance model for interfacial heat transfer, the evaporation-condensation model should be the Thermal Phase Change Model.

Lee model

This model is governed by the vapour transport equation, practically the liquid – vapour mass transfer (evaporation and condensation) is based on the equation below [29]:

$$\frac{\partial}{\partial t}(\alpha_{v}\rho_{v}) + \nabla \cdot (\alpha_{v}\rho_{v}\overrightarrow{V_{v}}) = \dot{m}_{lv} - \dot{m}_{vl}$$
 (1)

Where:

V = vapour phase

 α_v = volume fraction vapors

 $\rho_v = density vapors$

 $\overrightarrow{V_v}$ = vapours phase velocity

 \dot{m}_{vl} , $\dot{m}_{lv} = rates$ of mass transfer due to evaporation and condensation

If $T_1 > T_{sat}$ (evaporation)

$$\dot{m}_{lv} = coeff \cdot \alpha_l \ \rho_l \frac{(T_l - T_{sat})}{T_{sat}}$$
 (2)

If $T_v < T_{sat}$ (condensation)

$$\dot{m}_{vl} = coeff \cdot \alpha_v \ \rho_v \frac{(T_{sat} - T_v)}{T_{sat}} \eqno(3)$$

The coeff term represents a coefficient that must be found through simulations and can be interpreted as a relaxation time.

For a flat interface, the Hertz Knudsen formula provides the evaporation – condensation flux based on the kinetic theory:

$$F = \beta \sqrt{\frac{M}{2\pi RT_{sat}}} (P^* - P_{sat})$$
Where:

P = pressure

R = universal gas constant

 β = accomodation coefficient

 P^* = vapour partial pressure

The accommodation coefficient shows the portion of vapour molecules going into the liquid surface and absorbed by that surface.

The Clapeyron – Clausius equation relates the pressure to the temperature for saturation condition:

$$\frac{dP}{dT} = \frac{L}{T(v_v - v_l)}$$
Where: (5)

 v_v, v_l = the invers of the density for vapour and liquid

L = latent heat

Furthermore, it can be obtained the variation of temperature from variation of pressure close to the saturation condition.

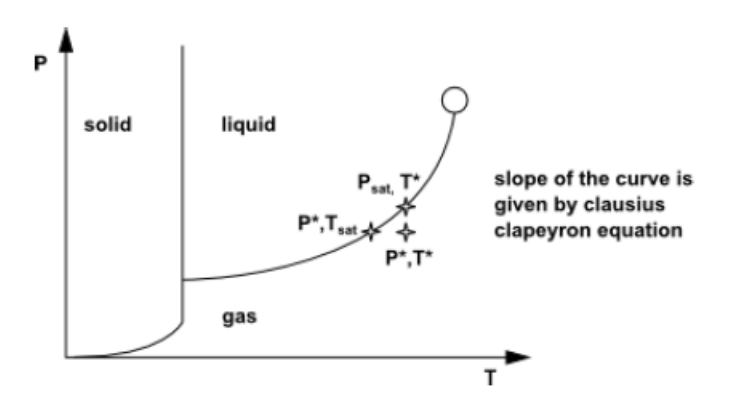


Fig. 5 – The phase diagram [29]

$$(P^* - P_{sat}) = -\frac{L}{T(v_v - v_l)} (T^* - T_{sat})$$
 (6)

Combining the Clapeyron – Clausius equation with the Hertz – Knudsen equation mentioned above results the following expression:

$$F = \beta \sqrt{\frac{M}{2\pi R T_{sat}}} L\left(\frac{\rho_{v} \rho_{l}}{\rho_{l} - \rho_{v}}\right) \frac{(T^{*} - T_{sat})}{T_{sat}}$$
(7)

Assuming that all droplets have the same diameter, the area density is assumed to have the following expression:

$$A_{i} = \frac{6\alpha_{v}\alpha_{l}}{d_{b}} \tag{8}$$

Where:

d_b – droplet diameter

The phase source term will have the following form:

$$FA_{i} = \frac{6}{d_{b}} \beta \sqrt{\frac{M}{2\pi RT_{sat}}} L\left(\frac{\rho_{v}\rho_{l}}{\rho_{l} - \rho_{v}}\right) \left[\alpha_{l}\rho_{l} \frac{(T^{*} - T_{sat})}{T_{sat}}\right]$$
(9)

Resulting the inverse of the relaxation time as follows:

$$coeff = \frac{6}{d_b} \beta \sqrt{\frac{M}{2\pi R T_{sat}}} L \left(\frac{\alpha_v \rho_v}{\rho_l - \rho_v}\right)$$
 (10)

This expression will be used as a source term in the conservation phase process. As this refers to the evaporation process, a similar formula is used to define the condensation process.

As the bubble diameter and accommodation coefficient are usually not very well known, coefficient coeff needs to be fine-tuned in accordance with the experimental data. This coefficient can take values form 0.1 and depending on the order of magnitude can go up to 10^3 .

2.2.2. Single phase models

These types of models propose the interior fluid as a mixture of water vapours and dry air. The second phase represented by the liquid water is not present. This assumption leads to a single set of equations, resulting in a reduction of the simulation time on one hand and a reduction in the computational need.

The condensation phenomenon is complex and therefore involves several parameters that require constant assessment. Furthermore, the building applications do not count the huge amounts of condensation as in the case of equipment such as condensers. Therefore, these single-phase models should be a simple and effective manner to simulate the condensation phenomenon inside buildings and vehicles by using lower requirements in computational resources and less time-consuming simulation need.

The single-phase model presented in the following pages is based on the International Energy Agency methodology. This was considered in previous studies conducted by Teodosiu

R. [30] which adjusted the model in order to predict the results based on experimental data. The same model was further developed by Ilie V. [31].

This model is based on the following simplifications:

- The mixture of dry air and water vapours represents a mixture of an idea gas
- The mixture is an incompressible gas and is recognized as a Newtonian fluid
- The interactions between the heat and mass transfer are negligible
- There are no chemical interactions between the species from the mixture
- The viscosity of the fluid is determined on the kinetic theory of gases for an ideal mixture
- Specific heat of the fluid is determined as in eq. (12)
- Thermal conductivity for mixture is determined based on the kinetic theory for idea gases
- Fluid density is determined based on the equation of state for the ideal gas by taking into account the temperature of humid air is the mass participation of each component, as can be seen in the formula below:

$$\rho = \frac{P}{RT \sum_{1}^{2} \frac{m'_{i}}{M'_{i}}}$$

$$\tag{11}$$

The formula involves the following parameters:

m'_i = molar mass fraction for each species

 M'_{i} = molar mass for each species

T = mixure temperature

P = mixure total pressure

R = universal gas constant

Specific heat of the species mixture:

$$c_{p} = \frac{\sum_{1}^{2} m_{i} c_{pi}}{m}$$
Where: (12)

 c_{pi} = represents the specific heat at constant pressure for each component

Humidity modelling

A new equation was integrated in the CFD model in order to take into account the water vapor transport. This equation was intended to deal with the conservation of water vapor mass fraction. Equation (13) describes the non-isothermal air flow:

$$\rho \frac{\partial}{\partial x_{i}} (u_{i} m_{i'}) + \frac{\partial}{\partial x_{i}} J_{i',i} = S_{i'}$$
(13)

Where:

 x_i = spatial coordonate

 u_i = velocity component on direction i

 $m_{i'}$ = water vapor mass fraction

 $J_{i',i}$ = water vapor diffusion flux

 $S_{ii} = source/sink term$

The first term from the left side represents the convective term, the second one is the diffusion term and the one on the right is the source or sink term.

Further on, the diffusive term in equation (13) integrates molecular and turbulent diffusion:

$$\frac{\partial}{\partial \mathbf{x_i}} \mathbf{J_{i',i}} = \rho \frac{\partial}{\partial \mathbf{x_i}} \left(\mathbf{D_{i'}} \frac{\partial \mathbf{m_{i'}}}{\partial \mathbf{x_i}} \right) - \frac{\partial}{\partial \mathbf{x_i}} \left(-\overline{\mathbf{u'_1}} \overline{\mathbf{m'_1}} \right) \tag{14}$$

Where:

 $D_{i\prime}$ = water vapor molecular diffusion coefficient

 $u'_{i}m'_{i}$ = turbulent mass flux of water vapors

 u'_{i} = velocity fluctuation

By taking into consideration Fick's first law, which refers to the diffusion due to concentration gradients through a diffusion coefficient, there is a need to determine the moisture diffusion coefficient. This was determined as follows:

$$D_{i'} = \frac{f\eta}{\rho} \tag{15}$$

$$D_{i,m} = 2.26e - 0.5 \cdot \frac{1}{P} \left(\frac{T}{273}\right)^{1.81}$$
 (16)

$$\frac{PD_{i,m}}{(P_{ca}P_{cb})^{1/3}(T_{ca}T_{cb})^{5/12}\left(\frac{1}{M_a} + \frac{1}{M_b}\right)^{1/2}} = a\left(\frac{T}{\sqrt{T_{ca}T_{cb}}}\right)^b$$
(17)

Going back to the turbulent diffusivity term in equation (14), the solutal turbulent diffusivity and the eddy viscosity were both part of the turbulent Schmidt number S_{ct} :

$$\left(-\overline{u'_{1}m'_{1}}\right) = \frac{\mu_{t}}{Sc_{t}} \frac{\partial m_{i'}}{\partial x} \tag{18}$$

$$Sc_{t} = \frac{\mu_{t}}{\rho D_{t}} \tag{19}$$

As a result, equation (13) results in the following form:

$$\rho \frac{\partial}{\partial x_{i}} (u_{i} m_{i'}) - \rho D_{i,m} \frac{\partial}{\partial x_{i}} \left(\frac{\partial m_{i'}}{\partial x_{i}} \right) - \frac{\partial}{\partial x_{i}} \left(\frac{\mu_{t}}{S c_{t}} \frac{\partial m_{i'}}{\partial x_{i}} \right) = S_{i'}$$
 (20)

For this study, the surface condensation is taken into consideration. Therefore, the following assumptions were made:

- The solid surfaces are impermeable, and no exchange is made with the outside air.
- The quantity of condensation is very low.
- The liquid drops are taken out from the computational domain.
- The thermophysical properties vary with mass fraction.

To start a condensation phenomenon, the solid surface needs to reach a temperature below the dew point temperature. Therefore, the assessment of temperature on the solid surface is a key factor in determining the condensation process. It is highly important to take into consideration the sensible heat transfer (conduction, convection, and radiation), as well as latent heat transfer of the solid surface in order to properly evaluate the surface temperature. The walls considered as monolayers are taken into account for heat transfer through conduction. Nonetheless, the radiation heat transfer was implemented based on the Surface-to-Surface model. This approach does not take into consideration the interior water vapours, considering the interior air as non-participative.

The International Energy Agency proposed the single-phase condensation process where the water vapours transport in air is generally determined by convective movement. Nonetheless, near walls regions the diffusion is more significant. Thus, in this model the cells next to the walls is behaving like a diffusion phenomenon as described in the formula below:

$$\phi_{\text{vap.cond}} = \beta (P_{\text{vap.air}} - P_{\text{vap.surface}})$$
 (21)

Where:

 β = proportionality coefficient (s/m)

 $P_{\text{vap.air}} = \text{vapour pressure indoor air}$

P_{vap.surface} – vapor pressure on the wall surface

The coefficient of proportionality (β) and the convective part results in the following formula:

$$\beta = \frac{h_c}{c_p RT \phi} \left[\frac{c_p RT \delta_p}{\lambda} \right]^{0.67}$$
 (22)

Where:

 h_c = convective heat transfer coefficient

 c_p = specific heat capacity of water vapors

 δ_p = water vapors permeability

With regards to building applications, equation (22) could be written as a formula depending on the convective heat transfer coefficient:

$$\beta = \frac{h_c \delta_p}{\lambda} = 7.4 \cdot 10^{-9} \cdot h_c \tag{23}$$

As previously mentioned, there are three region that can be highlighted for the interior flow:

- Viscous sublayer.
- Turbulent wall region.
- Outer turbulent region.

Therefore, for the region next to the wall, viscous sublayer, the convection equation can be written as follows:

$$\phi = h_c(T_w - T_{air}) \cdot S = h_c(T_F - T_{C0}) \cdot S_F$$
 (24)

Where:

 $T_{\rm w}$ = wall surface temperature

 $T_{air} = air temperature$

S = surface

 T_{C0} = temperature on the first barycentre cell (next to the wall)

 T_F = temperature on the face of the cell

Near the walls or the solid region, the viscous part is determined based on conduction heat transfer as the convection part has a lower impact. Therefore, the heat flux density based on the Fourier law (conduction) is determined as follows:

$$\varphi = -\lambda_{air} \overrightarrow{grad} \overrightarrow{Tn} = \lambda_{air} \left(\frac{\partial T}{\partial n} \right) = h_c (T_F - T_{C0})$$
 (25)

$$h_{c} = \frac{\lambda_{air}}{(T_{E} - T_{Co})} \left(\frac{\partial T}{\partial n} \right)$$
 (26)

Where:

 λ_{air} = thermal conductivity of the mixture

The temperature gradient is determined as follows:

$$\left(\frac{\partial T}{\partial n}\right) = \frac{(T_F - T_{C0})}{S_F} \cdot \alpha \tag{27}$$

Where α is further determined as follows:

$$\alpha = \frac{\overrightarrow{S_F} \cdot \overrightarrow{S_F}}{\overrightarrow{S_F} \cdot \overrightarrow{S_0}} \tag{28}$$

Where:

$$s_0 = (coord_F - coord_{C0)}$$
 (29)

The mass flow rate of water vapours which condensed on the solid surface $m_{\text{vap.cond}}$ for each face of the cell placed on the surface on the boundary is determined based on the following expression:

$$\dot{m}_{\text{vap.cond}} = \frac{dm_{\text{liq.surface}}}{dt}$$
 (30)

If $P_{vap} - P_{vap.sat} > 0$

$$\dot{m}_{liq.surface} = 7.4 \cdot 10^{-9} h_c S_{Fi} (P_{vap} - P_{vap.sat})$$
(31)

Else

$$\dot{\mathbf{m}}_{\text{lig.surface}} = \mathbf{0}$$
 (32)

Where:

 $\dot{m}_{lig,surface} = condensed vapour flux$

 $P_{\text{vap.sat}}$ = saturation pressure for the water vapours

 P_{vap} = partial pressure of water vapours

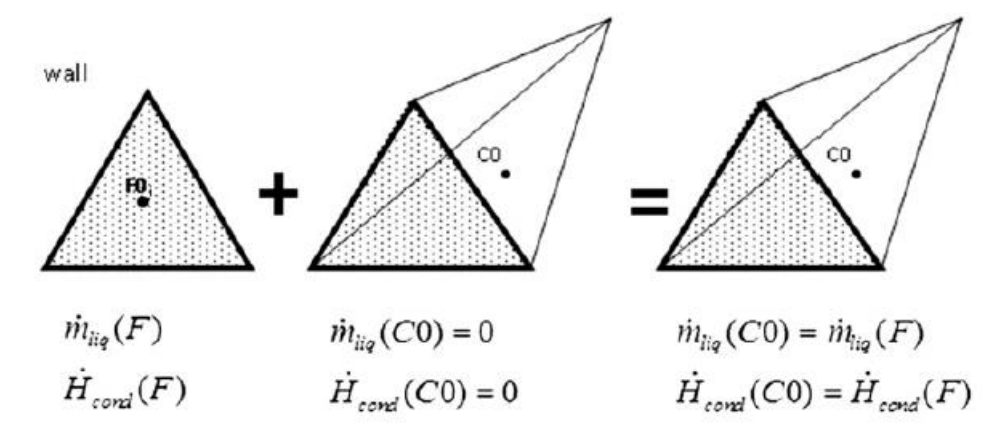


Fig. 6 – Exemplification of the mesh geometry near the wall

This method inserts a source term in the water vapour conservation mass which helps to remove the condensate flow rate from the computational domain in equation (13) and another sink term that intervenes in the energy balance equation and corresponds to the latent heat of vaporisation and sensible heat of the condensed water vapours.

$$\dot{H}_{cond} = \dot{m}_{vap.cond} \left[L_{vap} + c_p \cdot (T_{Fi} - T_{ref}) \right]$$
 (33)

Where:

 $\dot{H}_{cond} = total \ enthalpy \ of \ condensed \ water \ vapours$

 L_{vap} = water latent heat of vaporisation

 $T_{ref} = temperature \ reference$

3. Description of the numerical study

Similar to the real experimental approaches, the CFD techniques are capable of assessing the heat-air-moisture transfers at a global level in different applications [26]. Hence, for this reason, the present study focused on using a numerical approach in order to have a global picture of the evolution of the condensation process in time.

This part of the research programme involved the numerical approach of the condensation phenomenon taking place inside the vehicle's cabin, especially on the windshield region. As highlighted in the introduction part, the condensation phenomenon plays an important role in the driving range and the driving power of electric vehicles. These studies are meant to provide an insight with regards to the energy consumption and parameters on the windshield.

As the condensation process is still limited in the specialised literature in buildings [26], the same goes for the transportation industry. Thus, one of the goals of this research project is to provide an insight into this direction and take it one step further.

3.1. Geometry generation

As mentioned in the second report of this study, the geometry of a real scale vehicle compartment was constructed inside the climatic chamber at the Technical University of Civil Engineering Bucharest, at the Faculty of Building Services.

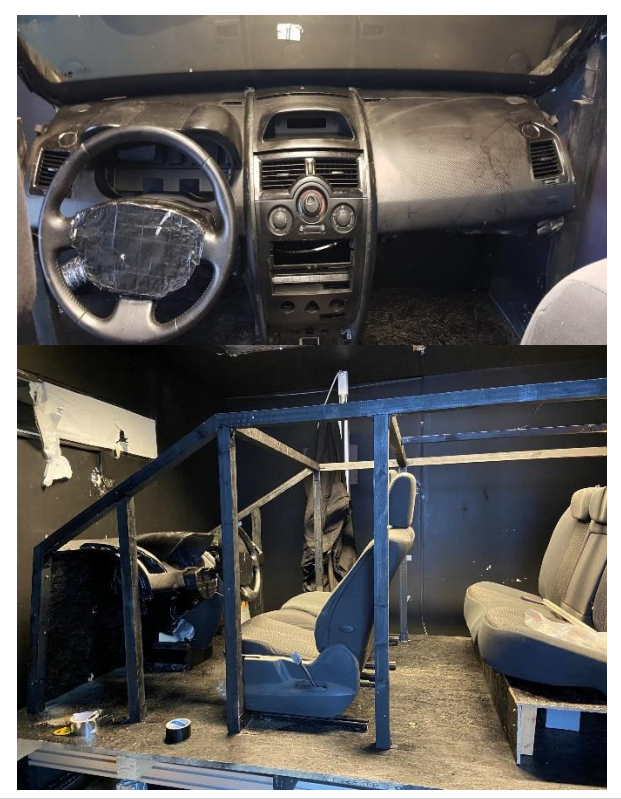








Fig. 7 – The experimental stand during different stages in its construction

Based on this experimental set-up, the geometrical characteristics were developed in 3D by using SolidWorks software. This part of the work was done in collaboration with Technical University Cluj – Napoca, more exactly coordinated by Profesor Florin Bode and Ph.D. student Titus Joldos. The model was transferred afterwards in Ansys Fluent where a mannequin, identical with the one from lab was introduced inside the cabin. The first sets of numerical determinations contained the mannequin at the interior of the vehicle's cabin. Nonetheless, due to high computerisation power and time restriction, the present study required a new mesh generation and a reduction in cell number. In consequence, the mannequin was taken out from the interior cabin.

3.2. Mesh generation

This part of the study was based on the geometrical characteristics previously highlighted. The mesh generation involved an unstructured mesh containing approx. 38 million of tetrahedral cells. These cells were further glued in a polyhedral mesh that resulted in 6.8 million cells. This reduction in cells greatly helped in CPU time requirement providing the incentives of obtaining results in a more restricted period of time without altering the final results. Multiple simulations were performed in order to make sure the results remains within the same range.

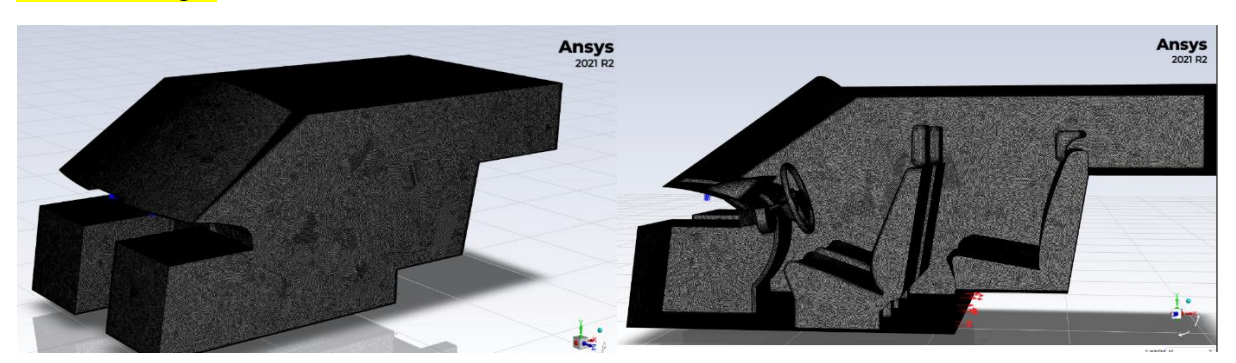


Fig. 8 – Mesh display

3.3. Numerical model

Since the fluid flows inside buildings are considered turbulent, the same goes for the ones that are taking place inside the passengers' compartments in vehicles. The analysed case needs to receive a turbulence model that considers the turbulent fluid flows inside the car on the one hand, but also all the phenomena that occur together with it, such as boundary layers, energy and mass transfer or phase change phenomenon. Thus, the chosen turbulence model must take into account all the phenomena involved in the real process, as well as to keep the simplicity levels and a reduced calculation time, without alteration of the results.

For this practice we used the $k-\omega$ SST model as it provides better results for the region close to the wall, as we were most interested in. The literature also proved that this $k-\omega$ SST model represents the best option for this case as it was shown through a comparison of the experimental and numerical results in several similar cases [32, 33].

In order to assess the condensation phenomenon, the species model was activated, and the interior fluid was set as a mixture of air and water vapours.

The model was analysed in transient set-up. For this study, it was chosen a step size of 0.5 s with a maximum number of iterations per step size of 20. This configuration proven to be the best solution in convergence, time management and results.

3.4. Radiation heat transfer

Previous report treated the importance of the radiation model in the final numerical results. According to our numerical simulations backed up by the findings in the literature, it seems that the implementation of the heat transfer through radiation can significantly change the indoor air temperature by 1-2 °C [34, 35]. For this study we chose the S2S radiation model as it is less time consuming and requires less computational resources. The model does not take into consideration the interior mixture of air and water vapours as participative in the heat radiation transfer. Nonetheless, it was proven that for interior water vapours concentrations that generally are very low in comparison with the ones in industry, considering the interior mixture as non-participative does not introduce errors in the numerical determinations [35].

3.5. Condensation process

As previously mentioned, the condensation phenomenon can be simulated through numerical approach by choosing a single-phase or a multi-phase approach. There are several pros and cons for each formulation. However, in this study the single-phase model was used. This model was proven to be very efficient in previous studies. The model based on the International Energy Agency was firstly used by R. Hohota [36] in hear research programme. Based on her model, V. Ilie [31] continued her approach by taking it a little bit further. He

moved the sensible and latent heat energy as a result of the condensation process from the centre of the fluid cell in the centre of the solid cell. This was accomplished by means of the UDF function as can be seen in the figure below.

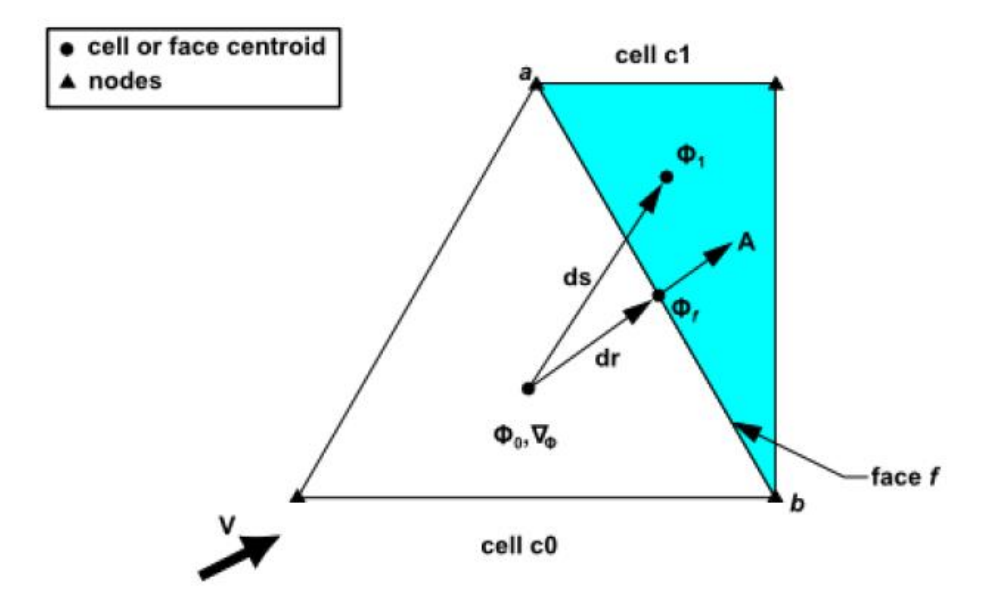


Fig. 9 – Description of the moving source term from one centre of the cell to the one next to it [37]

This new feature proved to be very useful for the new model as compared to the experimental results. Its outcome showed that the temperature prediction was improved by 0.3 °C compared to the previous model.

This study proposes to take even further the previous model and imposed the source terms only for the cells next to the windshield. Furthermore, the sink terms referring to the sensible and latent heat generation due to condensation phenomenon, instead of moving them from the centre of a cell to the other, this time they were imposed on the face of the cell that was in contact with the solid surface. Practically, through a skilful UDF usage the sink term was placed on a surface instead of a volume. This approach was used in order to bring the numerical model even closer to the real phenomenon.

3.6. Boundary conditions

The study was intended to analyse the interior conditions during the cold climate in the region of Bucharest city. Therefore, the initial conditions were set as follows: the exterior temperature 0 °C with a water vapours content of 0.8 g/kg. The initial conditions for the enclosed space were set for 0 °C and a humidity level of 30 g/kg of water vapours content. This humidity level was chosen at a greater level in order to highlight the condensation phenomenon on the vehicle's windshield. The air velocity introduced at the interior by using the demisting grids was first set to 12.5 m/s as in previous study after a thorough evaluation of the velocities presented for this case in the literature.

The temperature of the air introduced at the interior was set as variating in time in accordance with the experimental values found in the literature.

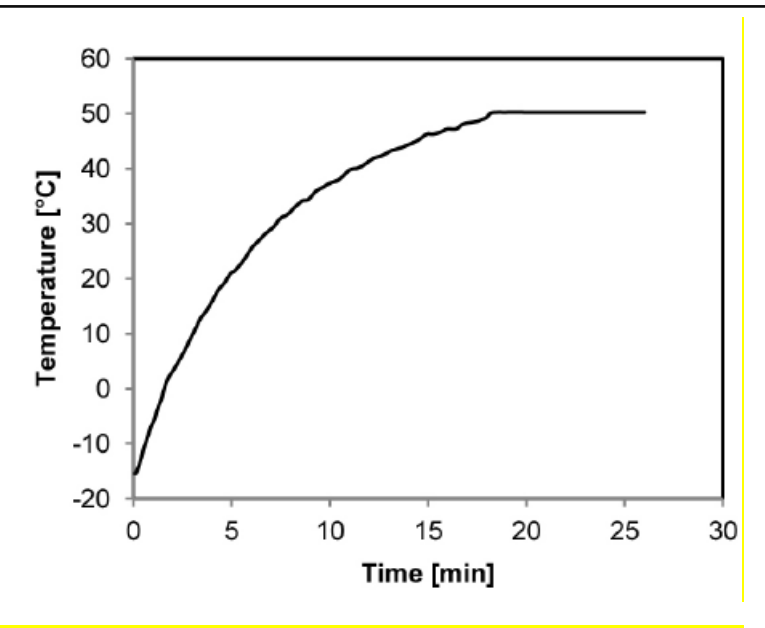


Fig. 10 – Variation of supply air temperature in time within the vehicle [38]

The properties of the materials were set in accordance with the ones found in the literature as can be seen in table below:

Table 1 – Material properties

	Density (kg/m3)	Specific heat (J/kg·K)	Thermal conductivity (W/m·K)	Thickness (mm)
Glazing surface ([39])	2500	750	0.8	4.9
Walls ([40])	1500	1000	0.2	10

The heat transfer through convection was set using the values determined in the literature, based on experimental approaches when the vehicles was found on stationary. These values are presented in Table 2.

Table 2 – Convection heat transfer coefficients [41]

	Stationary conditions
	Convection heat transfer coefficients
	$(W/m^2 \cdot K)$
Glazing surfaces on laterals	15
Windshield	20
Ceiling	3

3.7. Studied cases

This study was intended to determine the impact of the condensation phenomenon inside vehicles, especially on the windshield. Bearing this purpose in mind, several configurations were analysed in order to determine the impact of supply air velocity and

temperature on the condensation phenomenon and energy consumption. Therefore, the maximum air supply velocity was established at 12.5 m/s in previous studies based on a thorough assessment of the literature. Several cases were analysed by varying the air velocities at the inlet, more exactly, the 3 m/s, 6 m/s and 9 m/s were imposed.

Based on the 12.5 m/s velocity, the thermal power (W) of the heating system was established based on the following formula:

$$P_{th} = m \cdot c_p \cdot (T_{air} - T_{ext})$$
(34)

Where m represents the air flow introduced at the interior of the passenger compartment (kg/s), c_p is the specific heat (J/kg,°C) and T_{air} represents the temperature of the air introduced through the demisting grids (°C).

Another set of cases were analysed from the thermal power point of view. If the first set of cases involved a change in the air supply velocity, but the temperature of air remained the same for all four cases, this second type of cases involved a modification in supplied temperature, based on the new air velocity. The air flow was determined by multiplying the new air velocity with the area of the demisting grids. In these scenarios resulted new curves for temperature variation in time as can be seen in Fig. 11 below. The first temperature (blue line) represents the base of this study and was determined from the literature. Moreover, based on this temperature, the thermal power of the heating system was determined as previously explained. Temperature 2 (orange line), 3 (grey line) and 4 (yellow line) represent the new air supply temperatures, based on the same thermal power of the heating system.

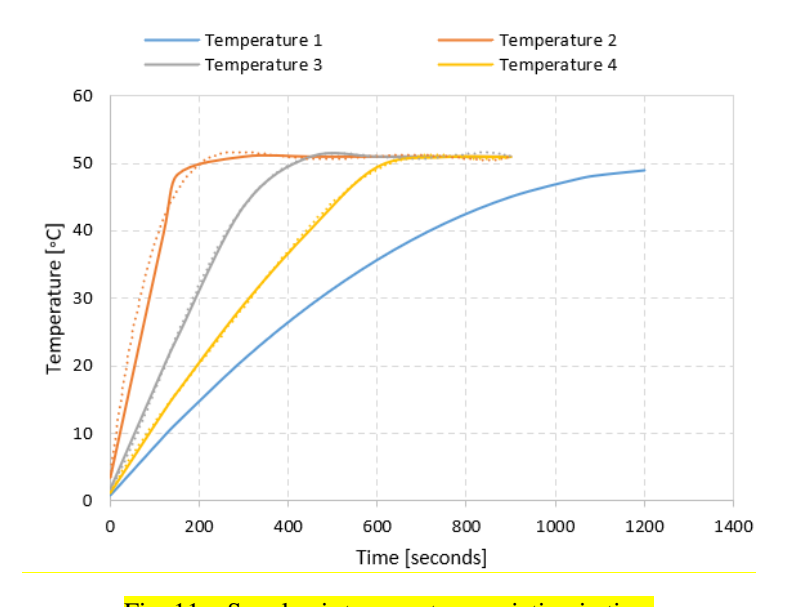


Fig. 11 – Supply air temperature variation in time

4. Results

The results were based on a transient determination for a period of 100 seconds. The seven cases were analysed in terms of mass flow rate of water vapours condensation, temperature of the windshield and energy consumption.

The heating power for the system determined through eq. (34) and the air velocity of 12.5 m/s resulted in a value of 0.2 kW for the first time step. However, for the two minutes simulation due to the inertia of the system, the thermal power was determined as being 2.1 kW. The value was reported in the literature as being the residual heat available in EV [10].

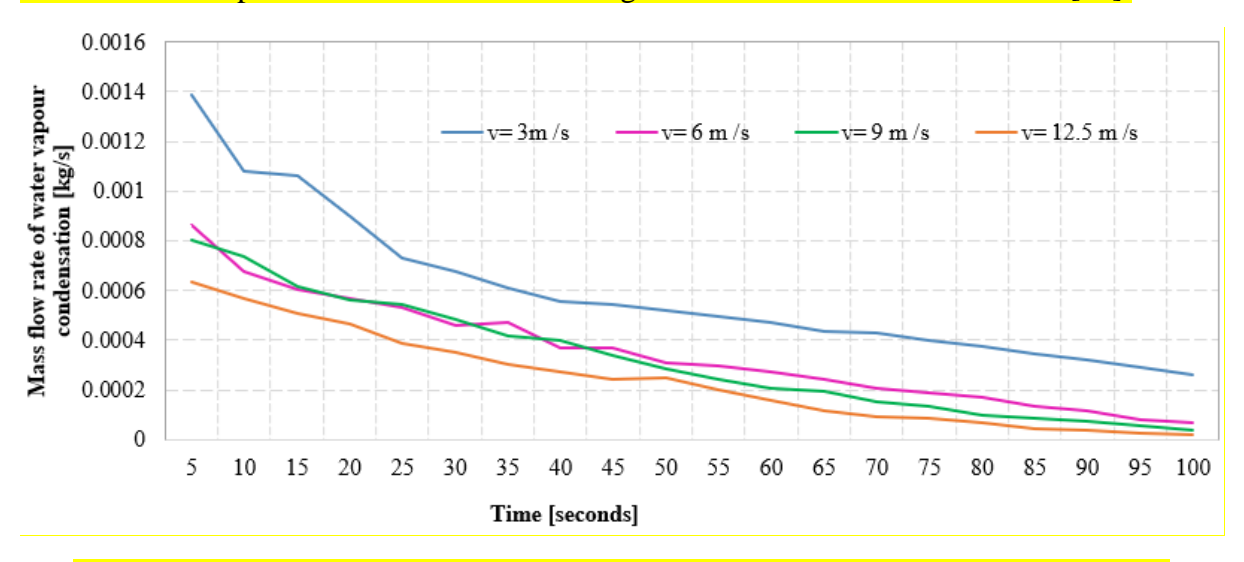


Fig. 12 – Mass flow rate of water vapours condensation for cases with the same air supply temperature

The first sets of results can be seen in Fig. 12, where the variation of the mass flow rate of water vapours condensation in time for the velocities of 12.5 m/s, 9 m/s, 6 m/s and 3 m/s for the supply air temperature using the blue line in Fig. 11 as described before, meaning the supply air temperature remains the same for all velocities. The graph shows that by introducing the air at the interior with a velocity of 12.5 m/s presents the lowest values of the mass flow rate of water vapours condensation, whilst an air velocity of 3 m/s produces the largest amount of condensation (around 1.4 g/s in comparison to 0.63 g/s for 12.5 m/s and 0.86 g/s and 0.81 g/s for the velocity of 0.6 m/s, respectively 9 m/s at 5 seconds) after the demisting system was turned on.

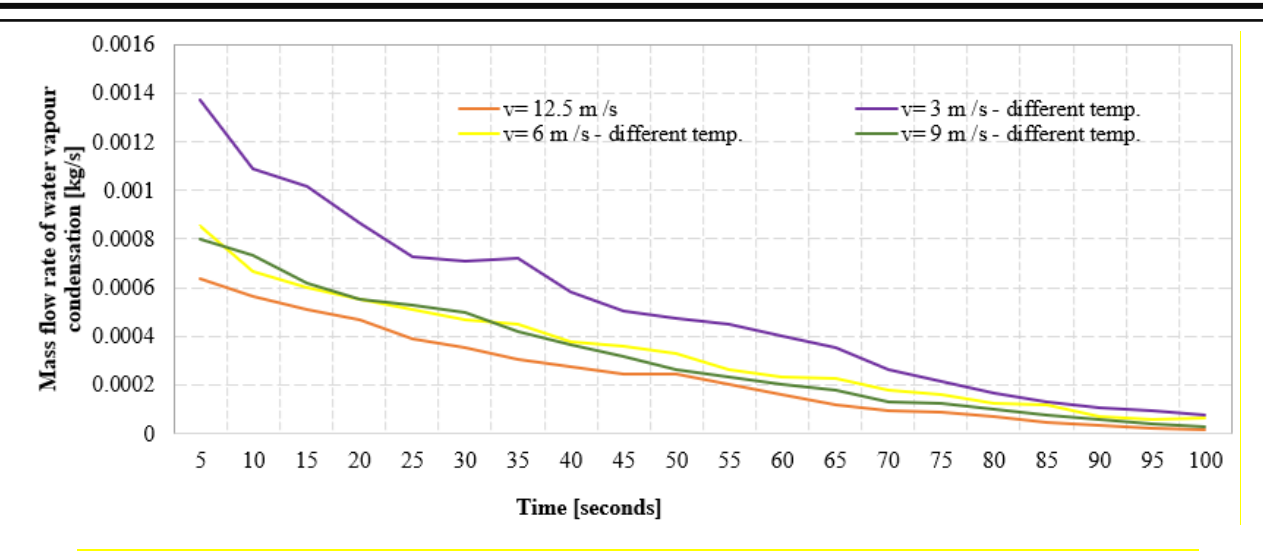


Fig. 13 - Mass flow rate of water vapours condensation for cases with variation of air supply temperature depending on the velocity

Fig. 13 shows another set of cases where the thermal power of the heating system determined for the air velocity of 12.5 m/s, was further varied with the air flow introduced at the interior. Practically, taking into account the same heating power, a lower air velocity resulted in a higher temperature of the air introduced inside the passenger's compartment. This graph shows that the air velocity of 12.5 m/s remains the best option in reducing the condensation phenomenon. Although the air velocity of 3 m/s introduces the air at a temperature of around 13 °C after 25 seconds in comparison with only 2 °C for the 12.5 m/s velocity, this still isn't enough do reduce the condensation phenomenon on the windshield. Moreover, after 60 seconds from the moment the demisting system is turned on, the mass flow rate of water vapours condensation drops significantly for the air velocities of 12.5 m/s, 9 m/s and 6 m/s, whilst for an air velocity of the supply air of 3 m/s the condensation phenomenon still presents significant values. More exactly, for 12.5 m/s the amount of condensation is 0.16 g/s whilst for 3 m/s the condensation phenomenon reaches 0.4 g/s. This represents a raise of 250 % in the mass flow water vapours condensation.

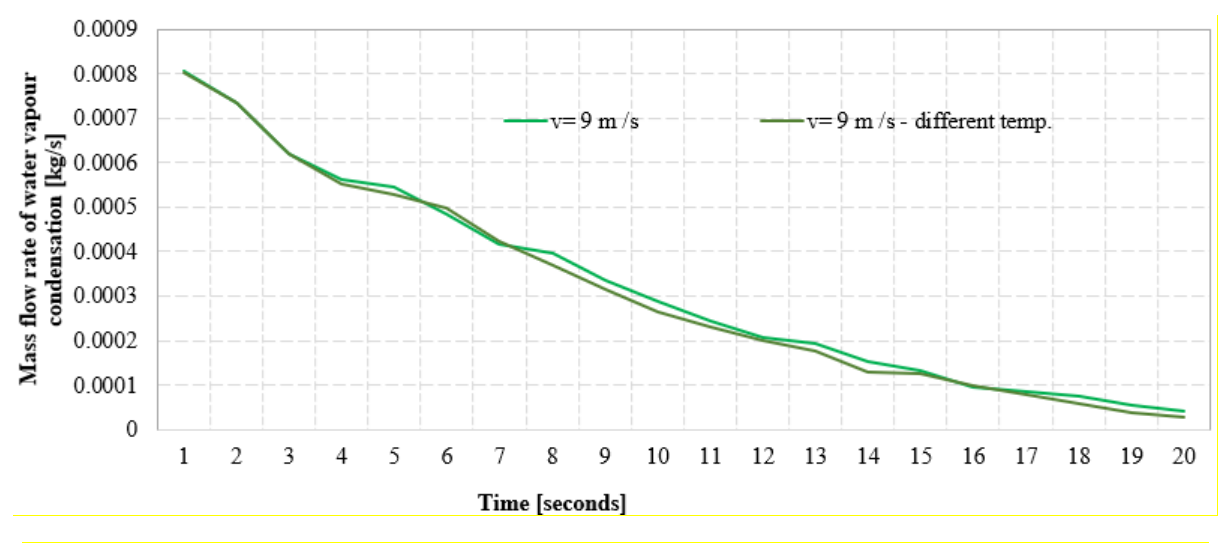


Fig. 14 – Comparison of mass flow rate of water vapours condensation for 9 m/s air supply at different thermal power of the heating system

Fig. 14 shows the comparison for the air supply velocity of 9 m/s when different air temperatures are introduced. The graph highlights a similarity between the two cases with

regards to the mass flow rate of water vapours condensation for both thermal powers. Basically, for this scenario, raising the temperature for the air supply cannot influence the condensation process. Moreover, maintaining the air supply temperature the same as for the 12.5 m/s results in a reduction of energy consumption of 0.19 kWh.

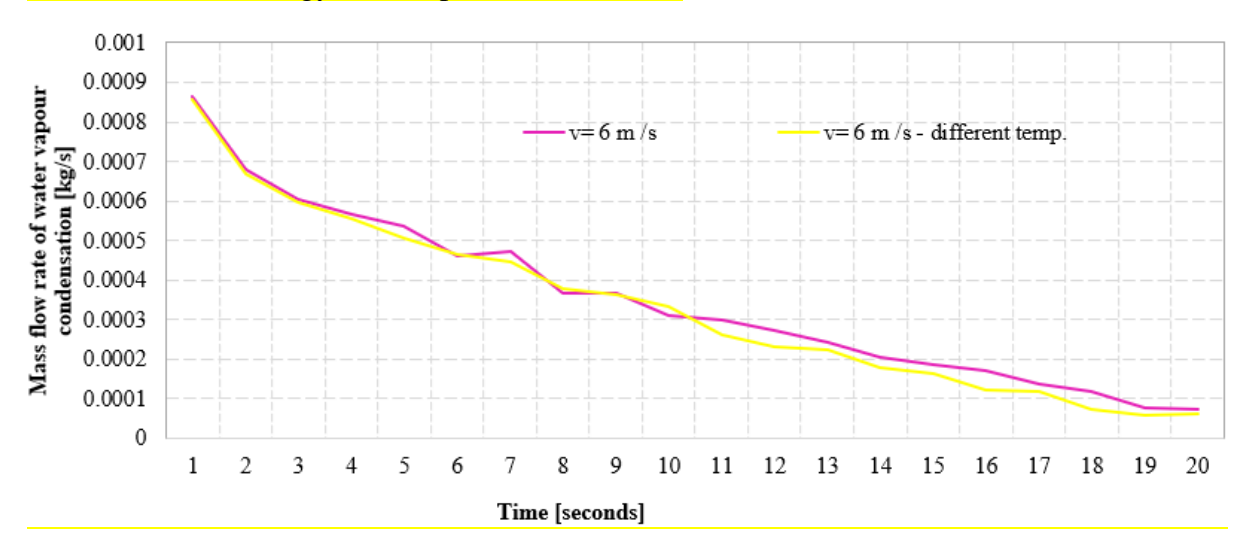


Fig. 15 – Comparison of mass flow rate of water vapours condensation for 6 m/s air supply at different thermal power of the heating system

Similar to Fig. 14, Fig. 15 shows the mass flow rate of water vapours condensation but for an air velocity of the supply air of 6 m/s. This graph maintains the supposition before that by changing the air temperature of the supply air is not sufficient to produce significant changes in the mass flow rate of water vapour condensation. This time, due to a reduction in air flow from 0.19 m³/s corresponding to 12.5 m/s to 0.09 m³/s for the air velocity of 6 m/s, the energy consumption drops by 0.29 kWh in comparison with the 0.19 kWh for the air velocity of the supply air of 9 m/s. This represents a reduction of approximately 66 %.

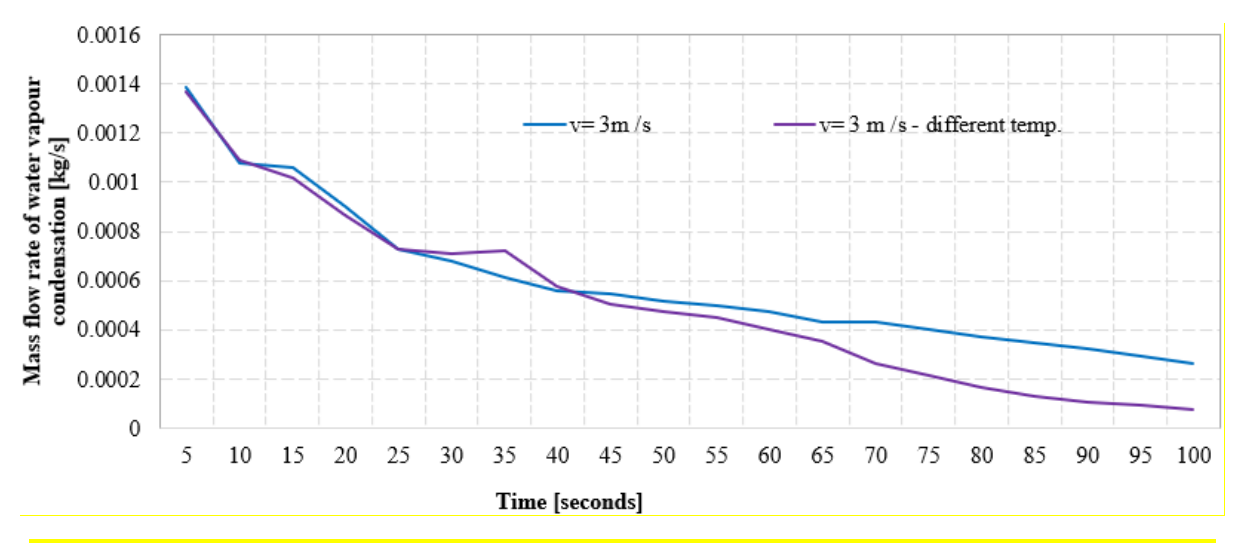


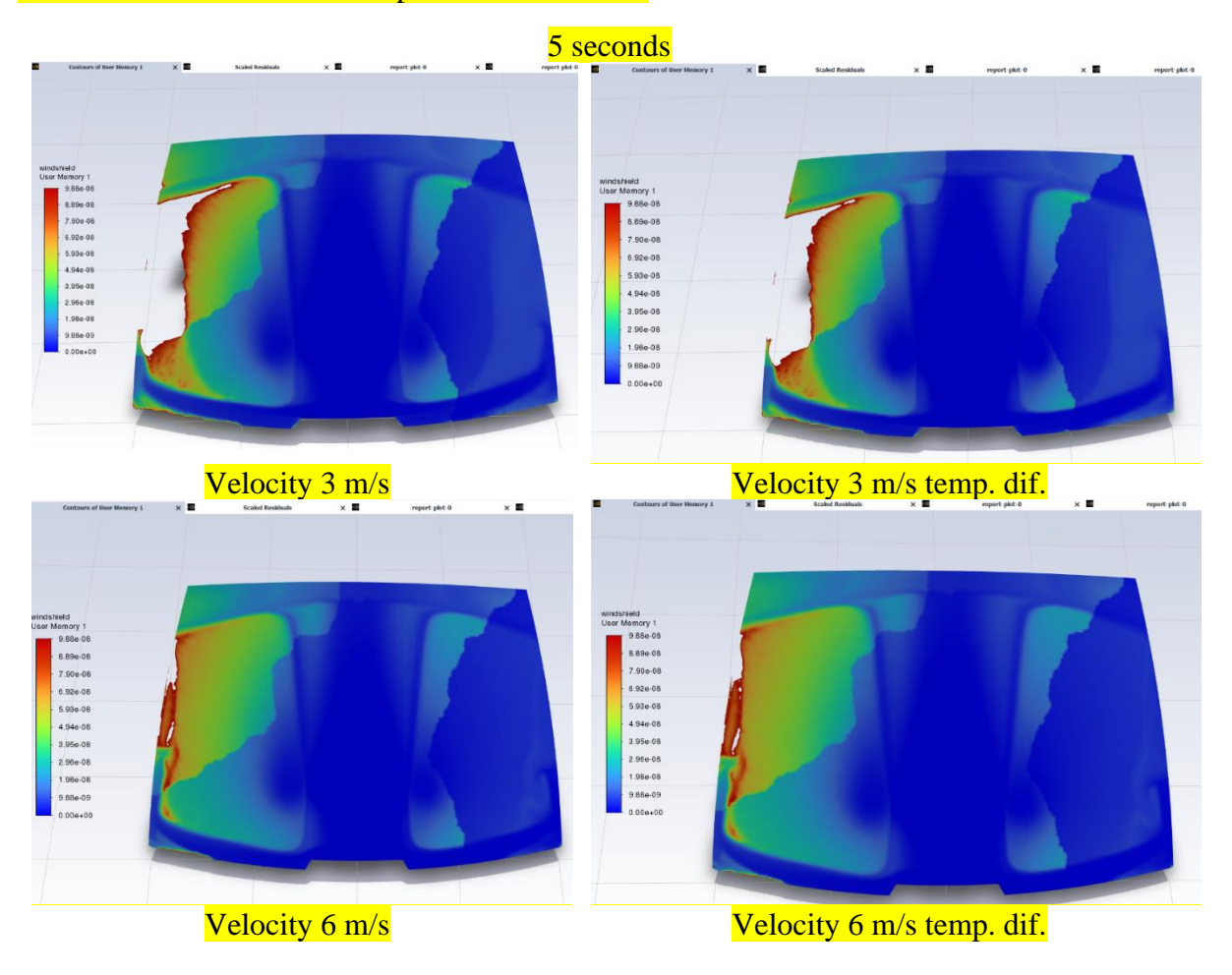
Fig. 16 – Comparison of mass flow rate of water vapours condensation for 3 m/s air supply at different thermal power of the heating system

The same goes for Fig. 16 which tackles the air velocity of supply air of 3 m/s. This drastically change in air velocity results also in changes in the mass flow rate of water vapours condensation. Starting after 60 seconds, a big gap starts to become visible between the air flow of 3 m/s with the supply air temperatures of 12.5 m/s and the 3 m/s with the corresponding

temperatures of the thermal power system. The energy difference between the scenarios is 0.6 Wh. This energy introduced through the supply air leads to a decrease in mass flow rate of water vapours condensation of 0.186 g/s, meaning a reduction of 93% of the mass flow rate of water vapours condensation. As the battery capacity of EV nowadays is around 70 kWh [6, 42] this energy raise in energy consumption in order to reduce the mass flow rate of water vapours condensation represents only 0.85 %.

It is important to mention as well in impact of the supply air flow. Increasing the ventilation air flow in order to lower the humidity levels and maintain the sufficient indoor temperature above the dew point crates a vicious circle that includes a raise in the energy cost [43].

The results mentioned above are also supported by the contours of the windshield for the mass flow rate of water vapours condensation.



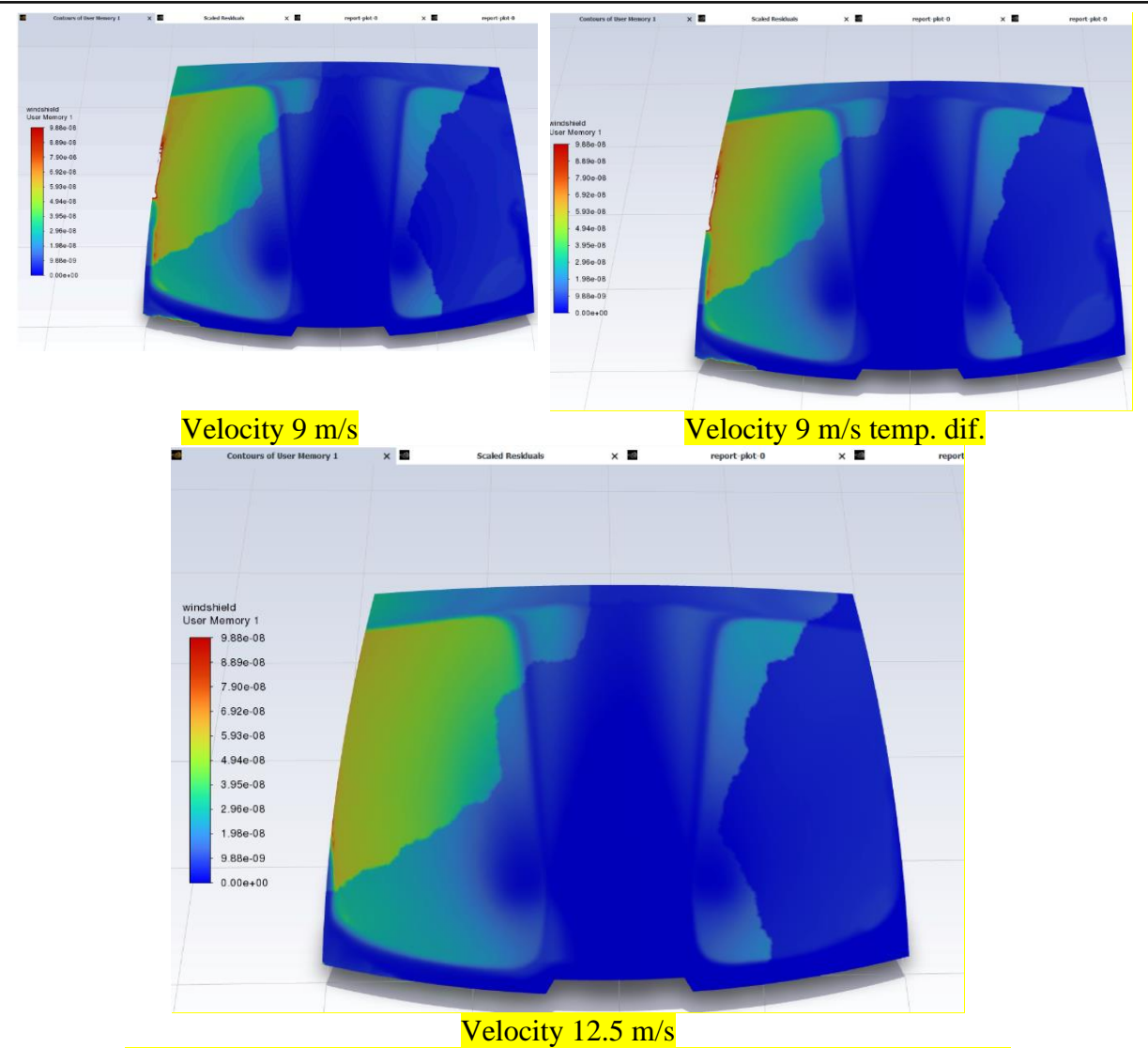
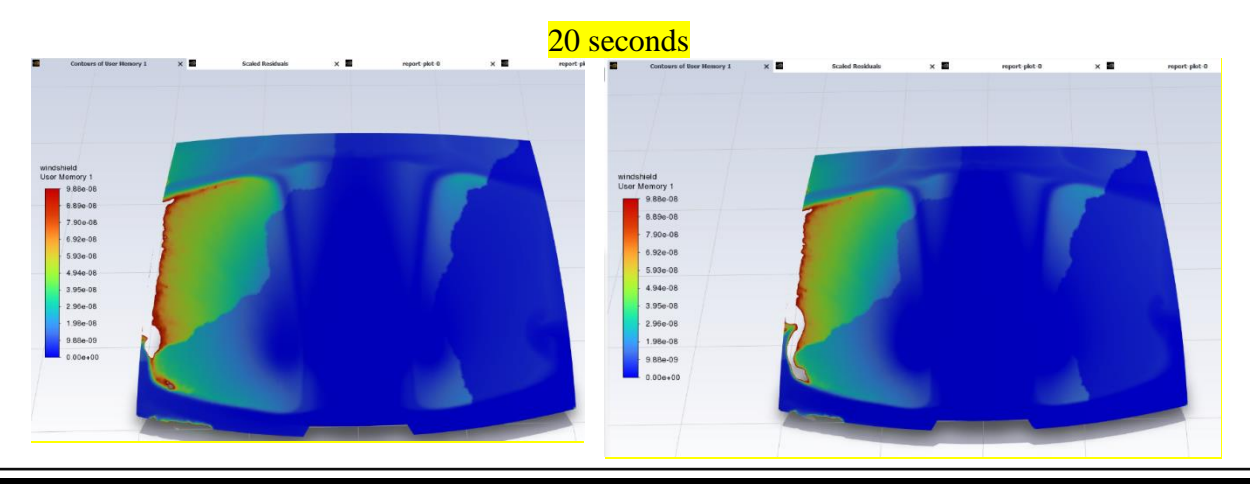


Fig. 17 – Mass flow rate of water vapours condensation windshield contour at 5 seconds

As supported by the general graphs below, the condensation phenomenon taking place on the windshield on the vehicle is showcased in Fig. 17 at 5 seconds after the demisting systems is set on. The contours show that the mass flow rate of water vapours condensation is lowest for the velocity of 12.5 m/s and it raises as the supply air velocity drops. Moreover, there are no significant visible differences between the scenarios with the same thermal power and the ones where the thermal power drops.



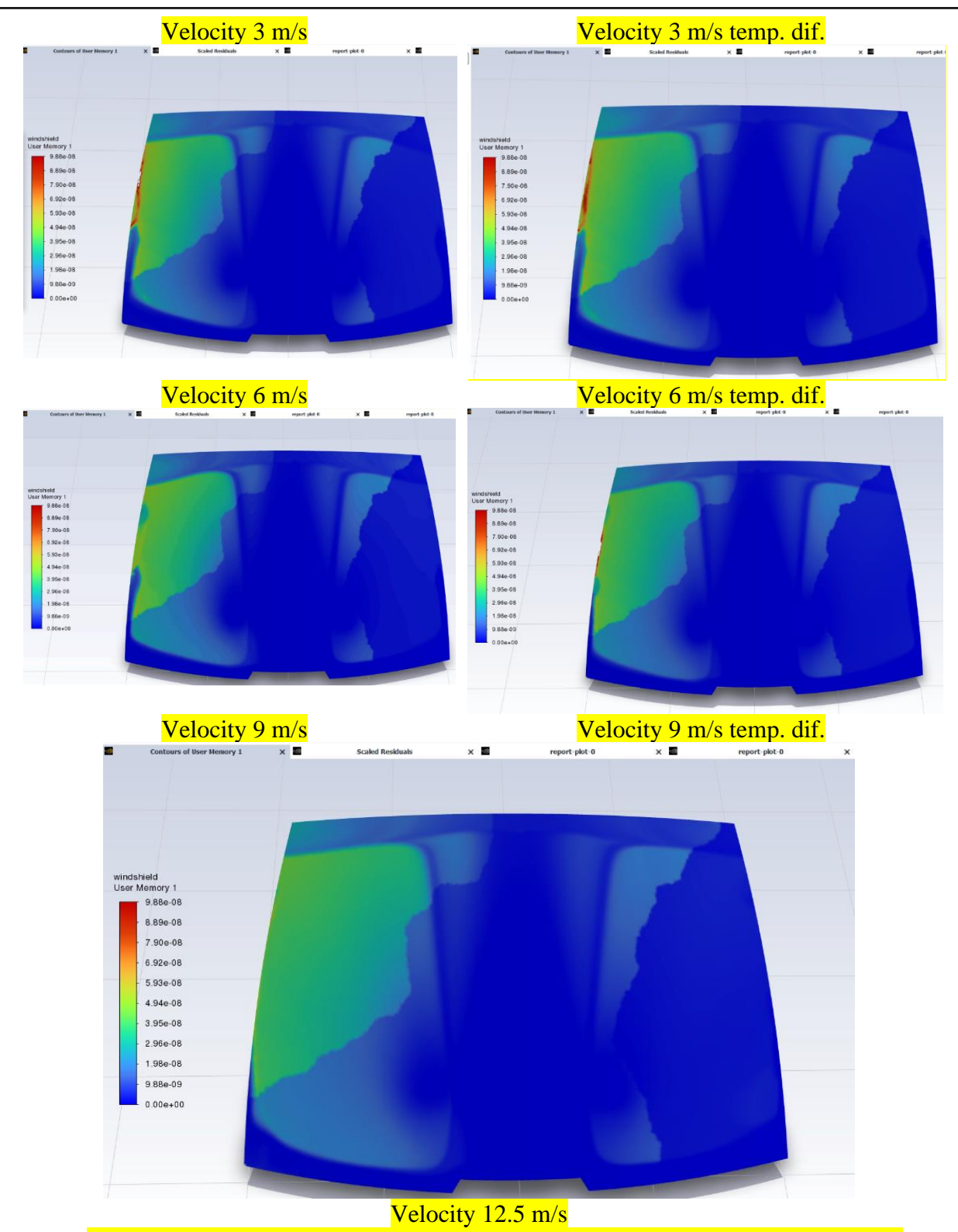
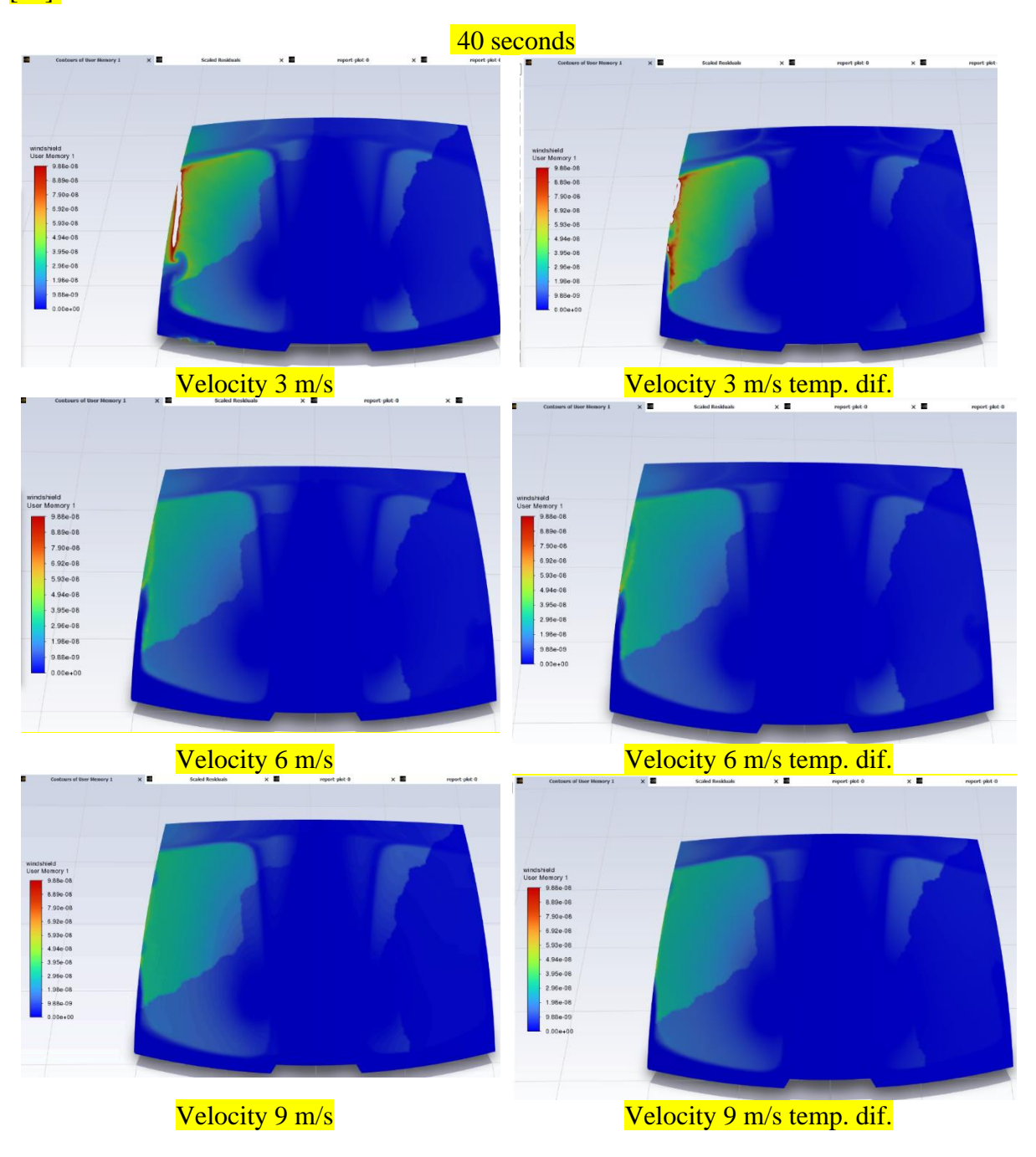


Fig. 18 – Mass flow rate of water vapours condensation windshield contour at 20 seconds

Fig. 18 showcases the evolution of the mass flow rate of water vapours condensation after 20 seconds of demisting system utilisation. This time step highlights the fact that the condensation phenomenon on the windshield is restricted in comparison with previous time step, meaning that the condensation starts to reduce its impact. Nonetheless, the air velocity of the supply air of 3 m/s still has a higher influence on the condensation process. Furthermore, it can be seen that for the right part of the windshield, the condensation phenomenon is less

significant than the one on the left part. This result expresses the findings in the literature which states that the driver' side benefits from more visibility and less condensation is general [8, 21]. Moreover, the legislation shows that this is highly important as the driver' side needs to be completely clear of any condensation process after 20 minutes of the demisting grids usage [14].



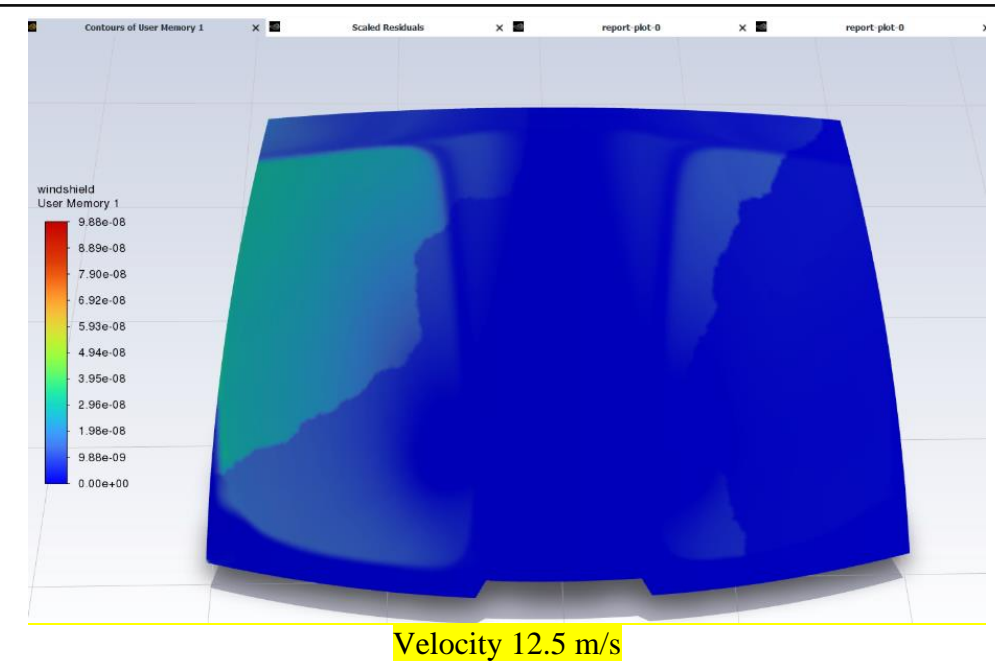
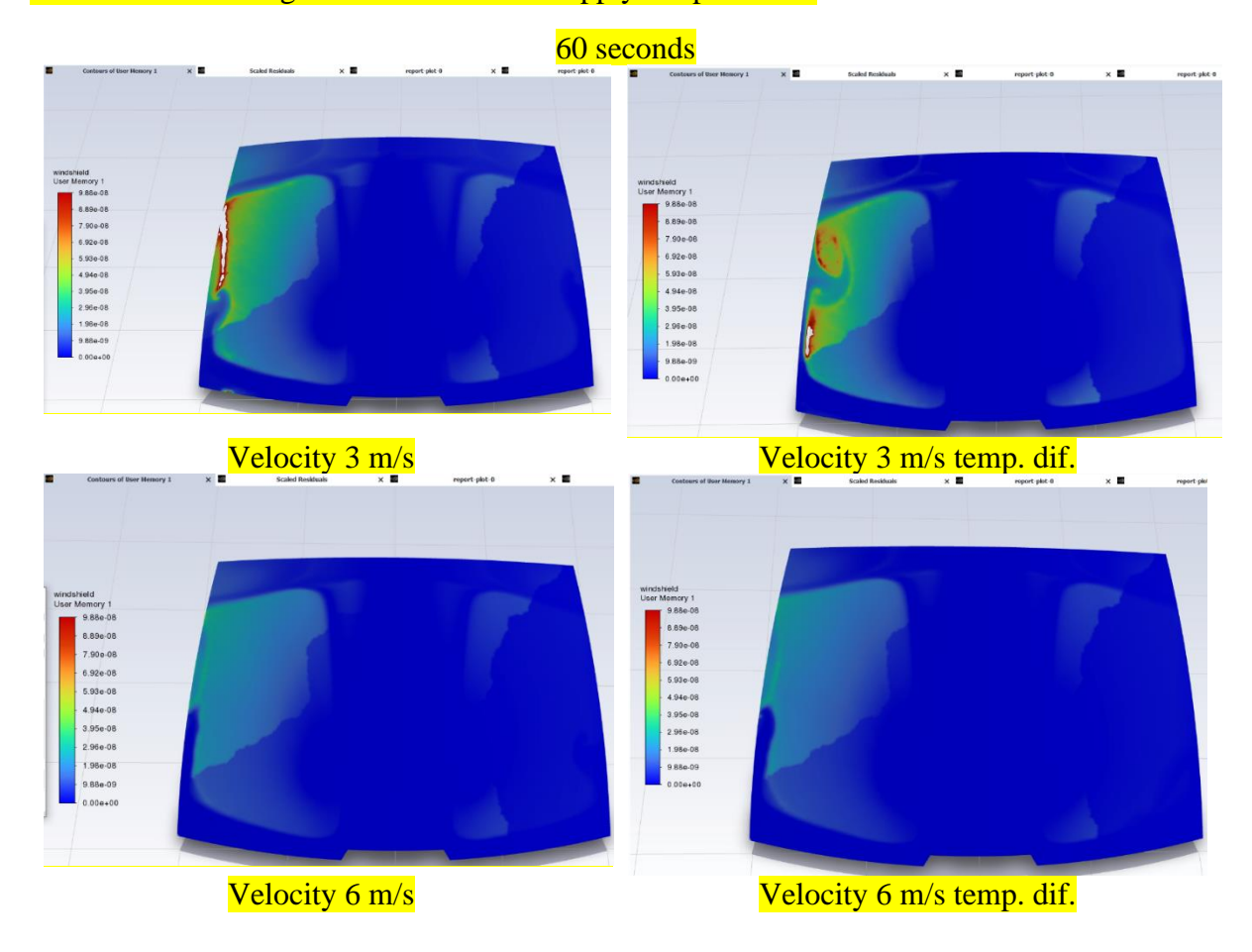


Fig. 19 – Mass flow rate of water vapours condensation windshield contour at 40 seconds

After 40 seconds of demisting systems usage some differences between the condensation process start to be seen at the air supply at 3 m/s in comparison with the 3 m/s and a higher air supply temperature. The area covered by the water condensation process starts to lower. The same goes for the other air supply temperatures.



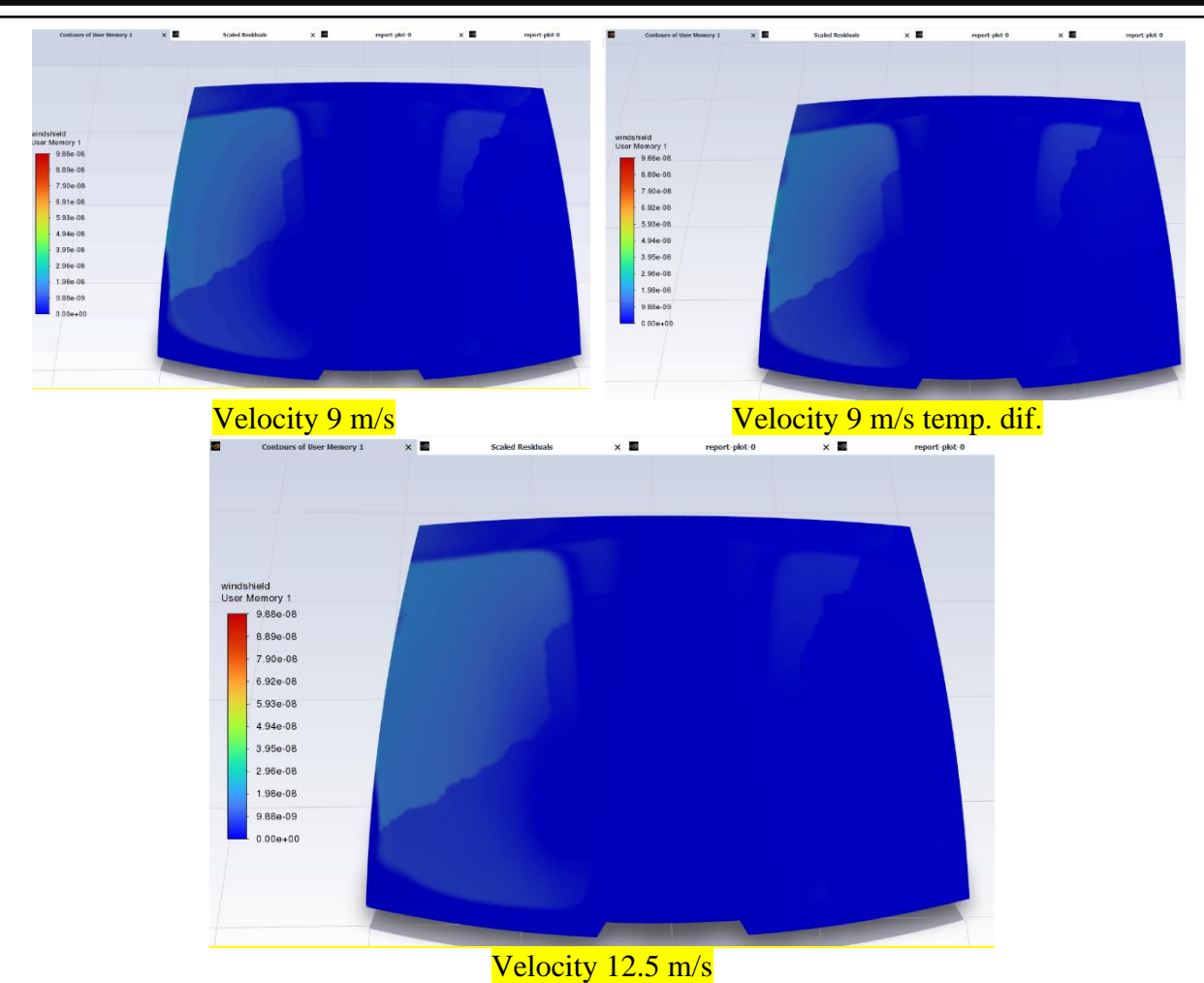
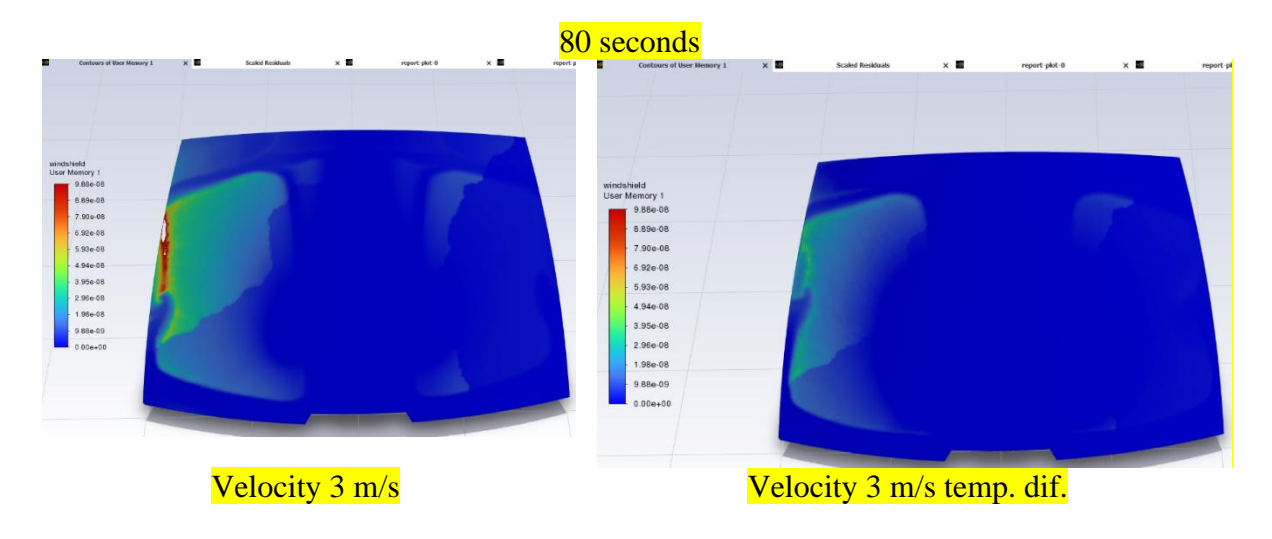


Fig. 20 – Mass flow rate of water vapours condensation windshield contour at 60 seconds

After 60 seconds it can be seen that the condensation starts to become less and less significant for all velocities and air temperatures. For the air velocity supply of 12.5 m/s the driver area is almost clear. The same goes for the air velocities of 9 m/s.



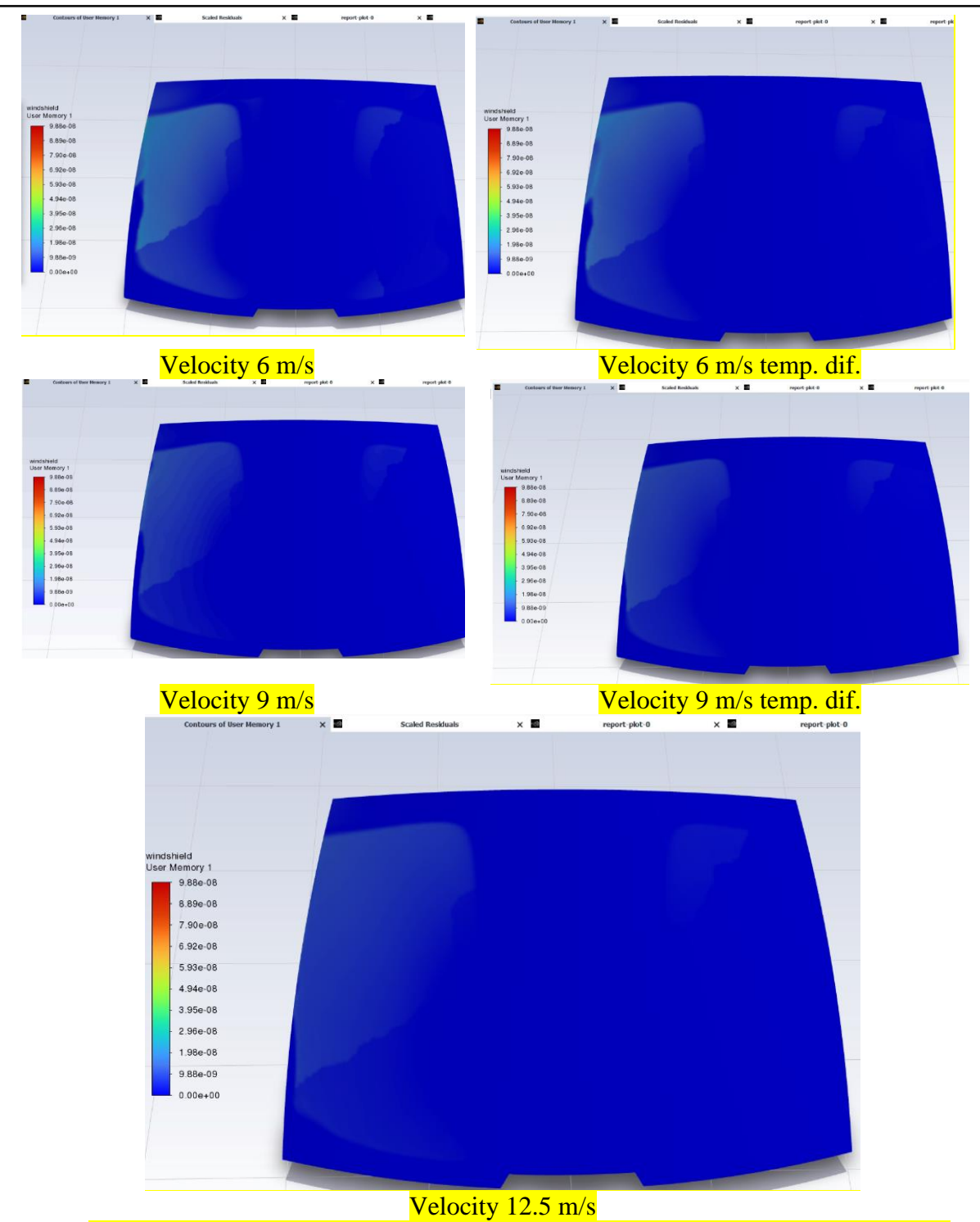


Fig. 21 – Mass flow rate of water vapours condensation windshield contour at 80 seconds

After 80 seconds of having the demisting system in function it can be seen in Fig. 21 that the condensation phenomenon is almost done for the air velocities of 9 m/s and 12 m/s regardless of the heating power of the system. Moreover, it also loses its impact for the air velocity of 3 m/s. However, for the air velocity of 3 m/s with the lowest power of the thermal system it can be seen that the condensation phenomenon still continues to have the highest impact.

100 seconds

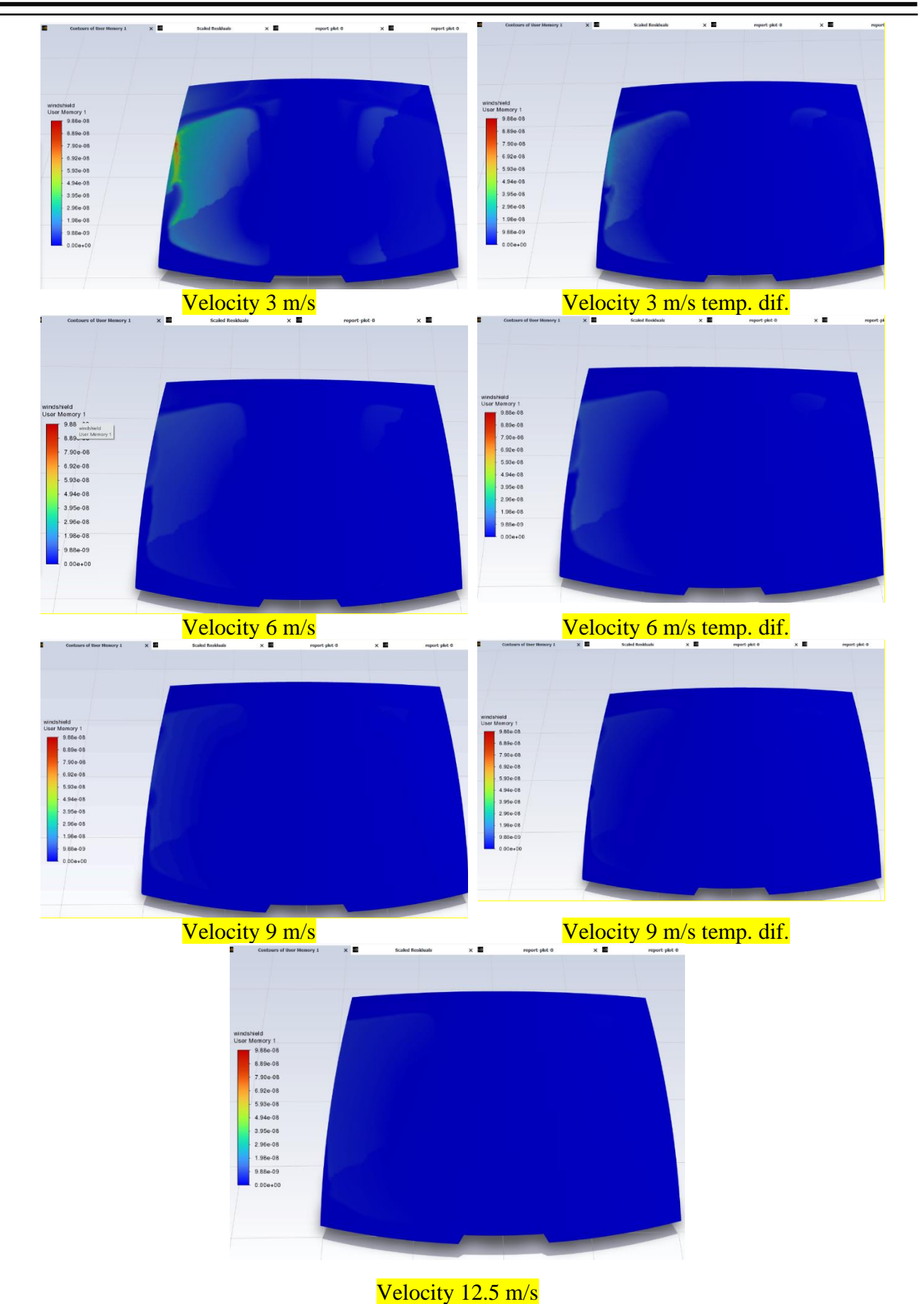
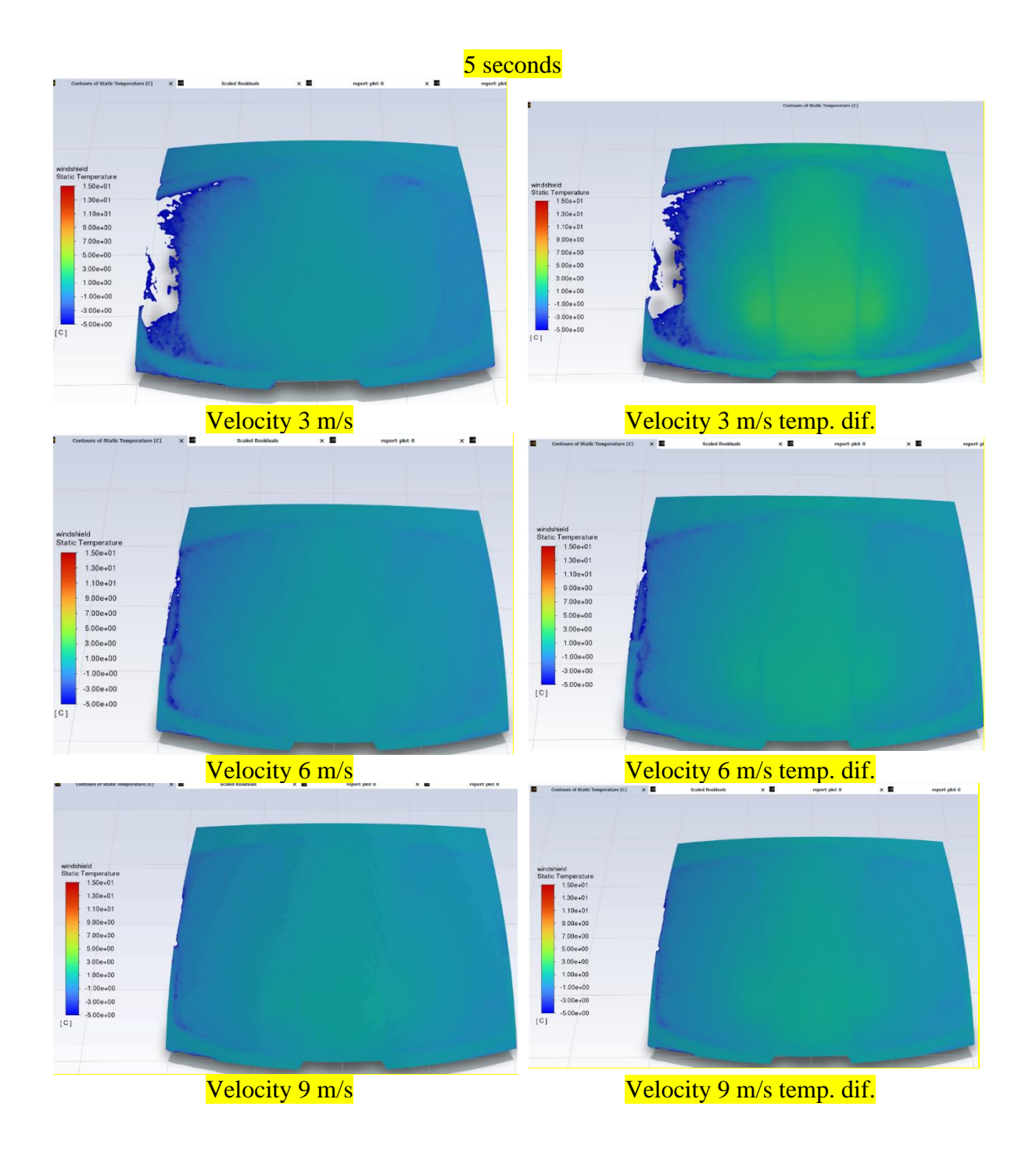
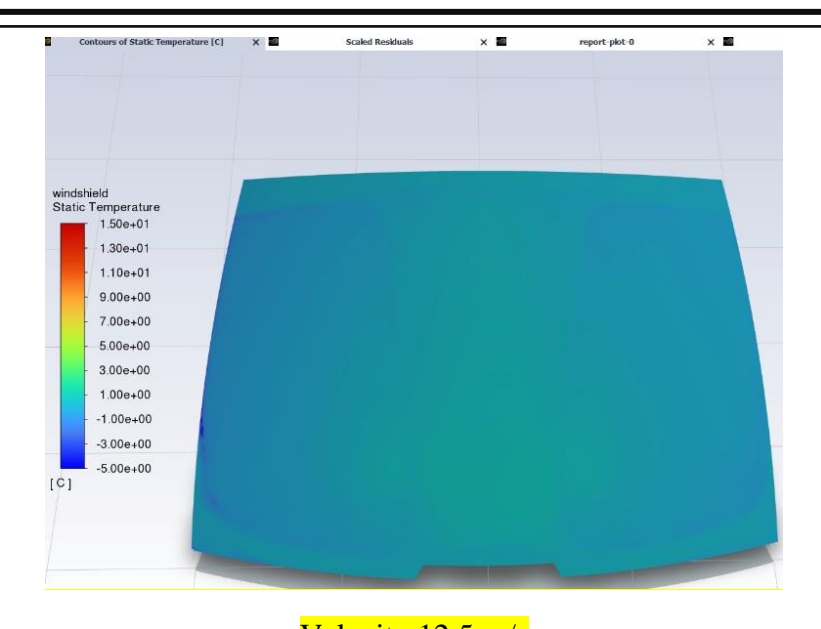


Fig. 22 – Mass flow rate of water vapours condensation windshield contour at 100 seconds

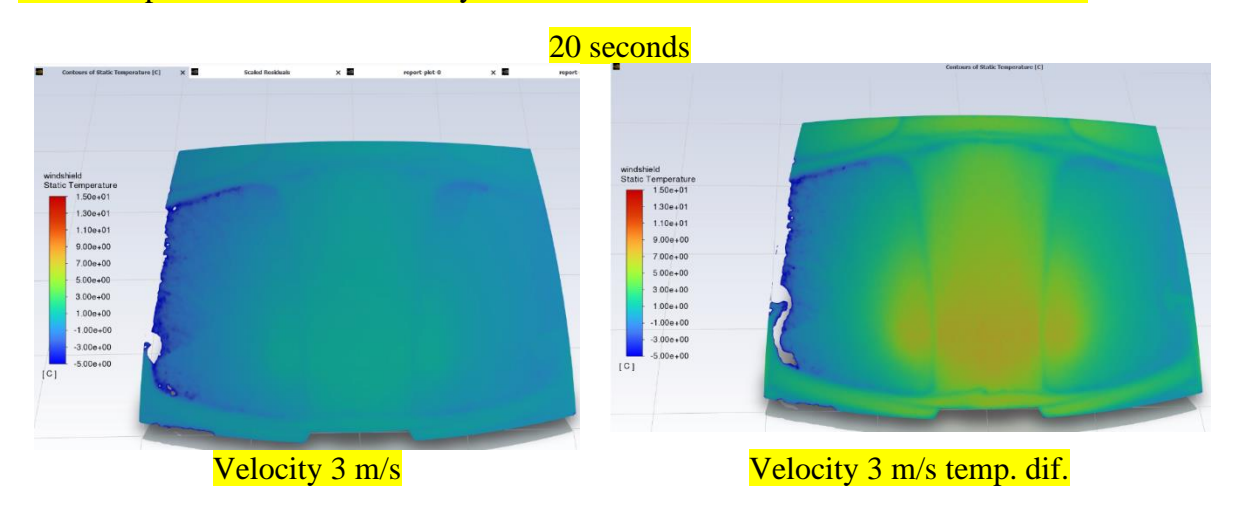
Fig. 22 shows that after 1 minute and 40 seconds the demisting system manages to clear all windshield area for the air velocity of the supply air of 12.5 m/s. However, the air velocity of 9 m/s and 6 m/s regardless of the air temperature of the supply air still have some areas that need to be addressed. The condensation process for the air velocity of 3 m/s at different temperatures is shown now in full display.





Velocity 12.5 m/s
Fig. 23 – Temperature contour on the windshield at 5 seconds

These new sets of graphs in Fig. 23 showcase the temperature contours on the windshield after 5 seconds of demisting grids usage. The first scenarios with the air velocity of 3 m/s of the supply air show an interesting phenomenon that takes place together with the condensation. As previously mentioned in the condensation model, a sink term is introduced in order to simulate the sensible and latent heat transfer that takes place together with the vaporisation and condensation phenomenon. Therefore, it can be seen that for the air velocity of 3 m/s when the condensation phenomenon takes place, a drop in the temperature takes place also. This leading to the idea that even though the condensation phenomenon produces a heat release, the heat release is further leading to an increase in heat transfer phenomenon, more exactly the temperature difference leads to an increase in heat loss as dictated by Newton's law. This phenomenon is extremely visible for the air velocities of 3 m/s and 6 m/s.



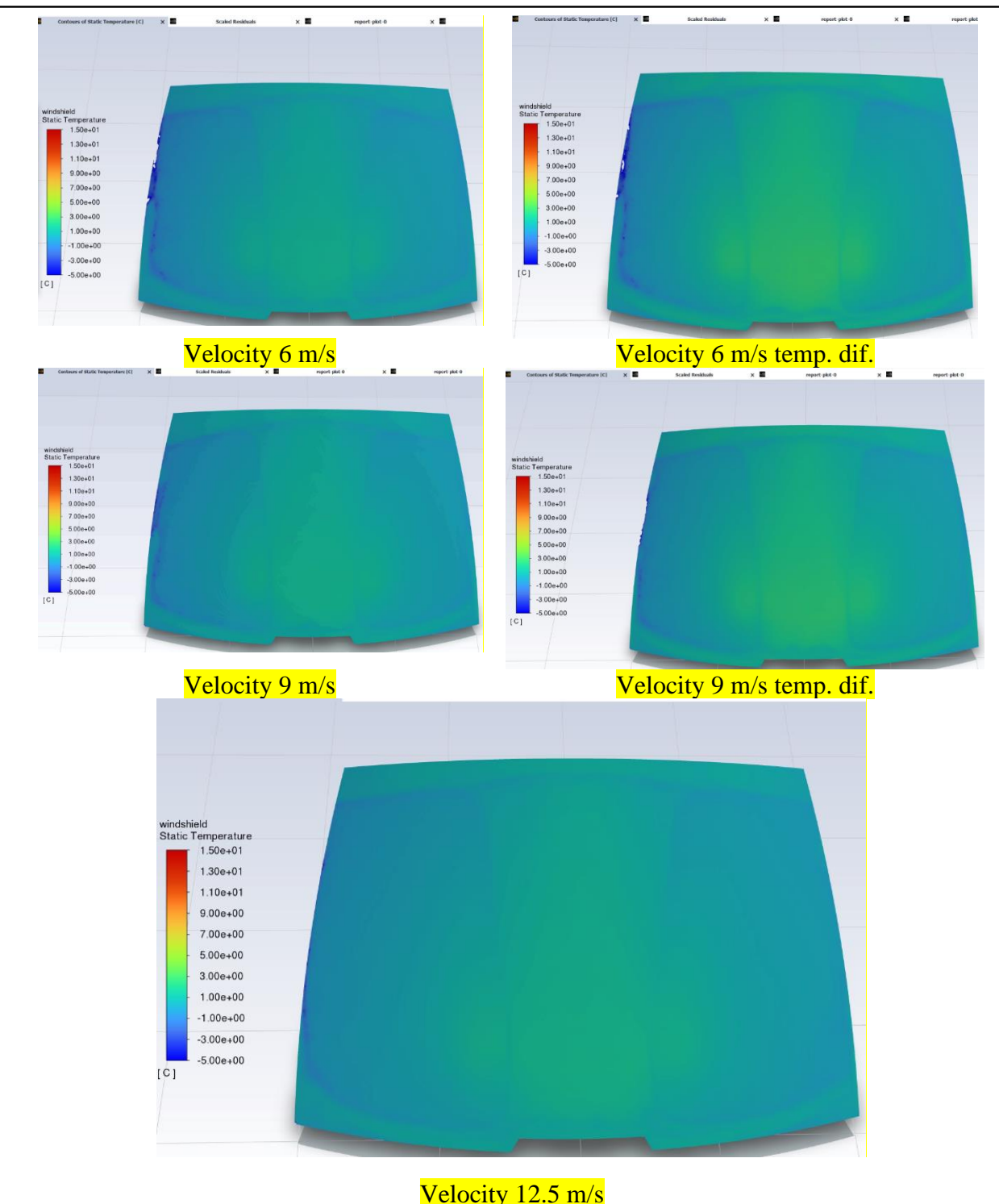
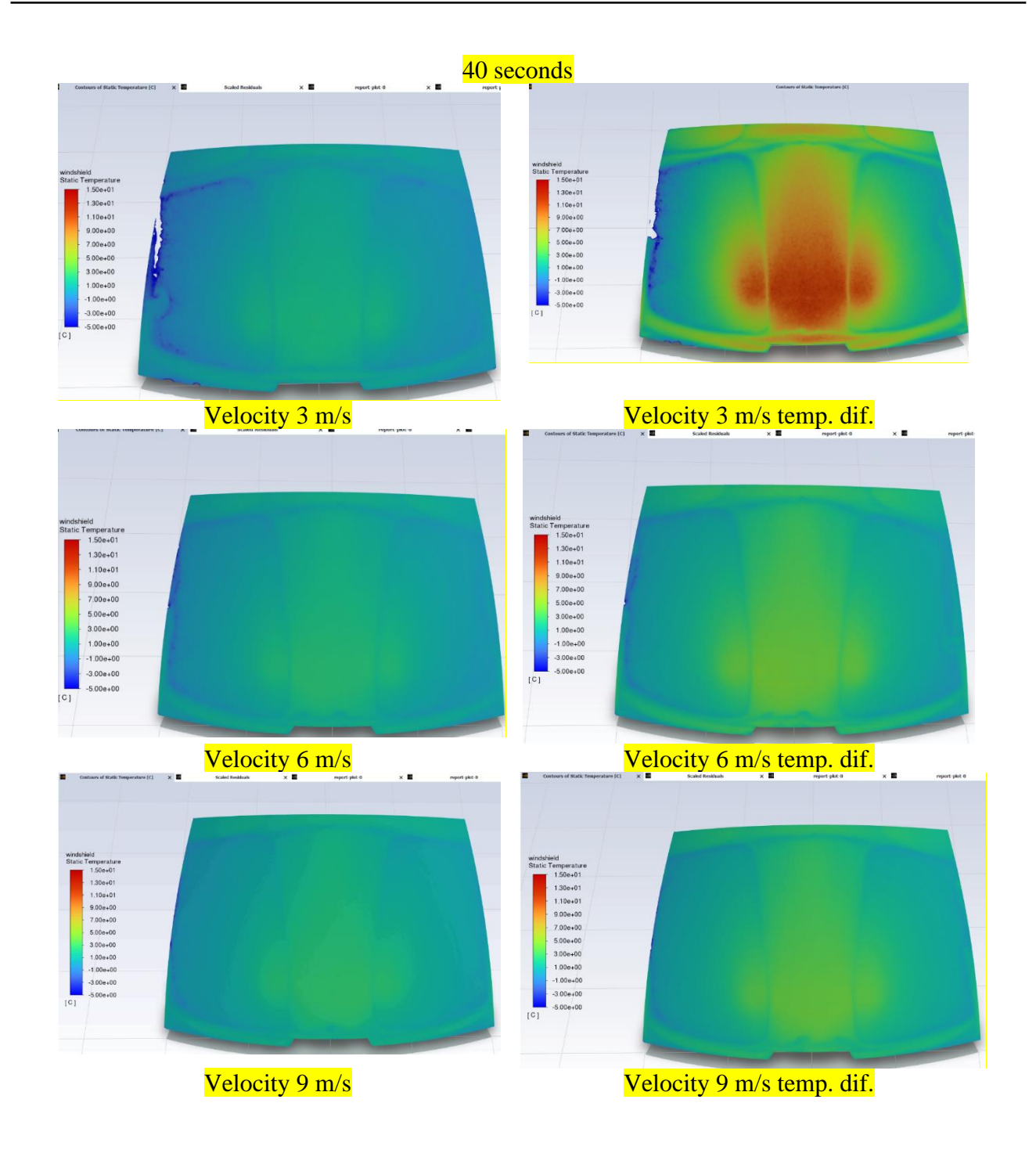
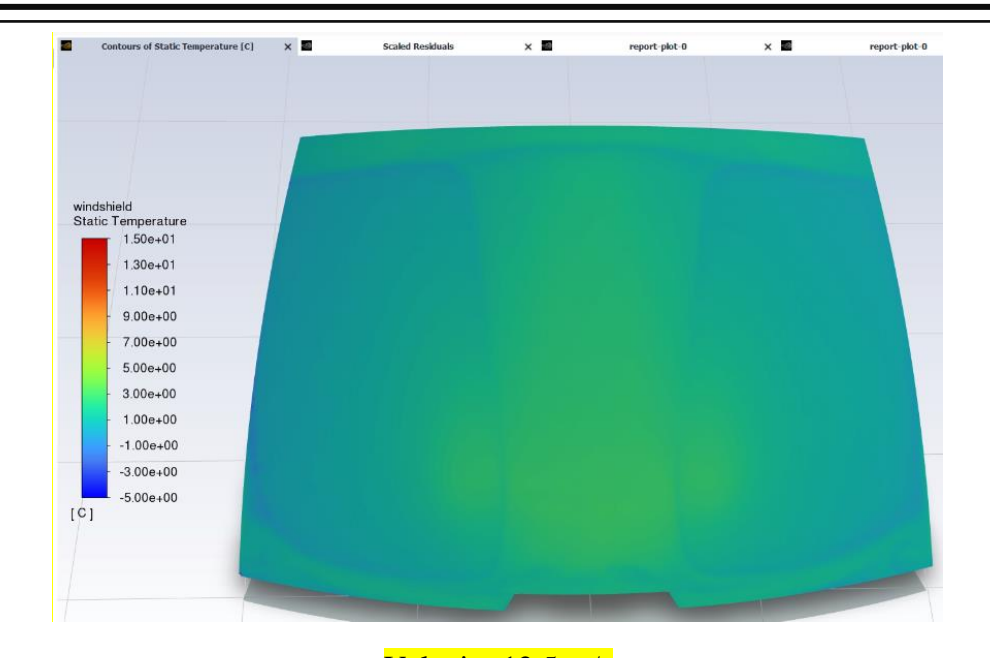


Fig. 24 – Temperature contour on the windshield at 20 seconds

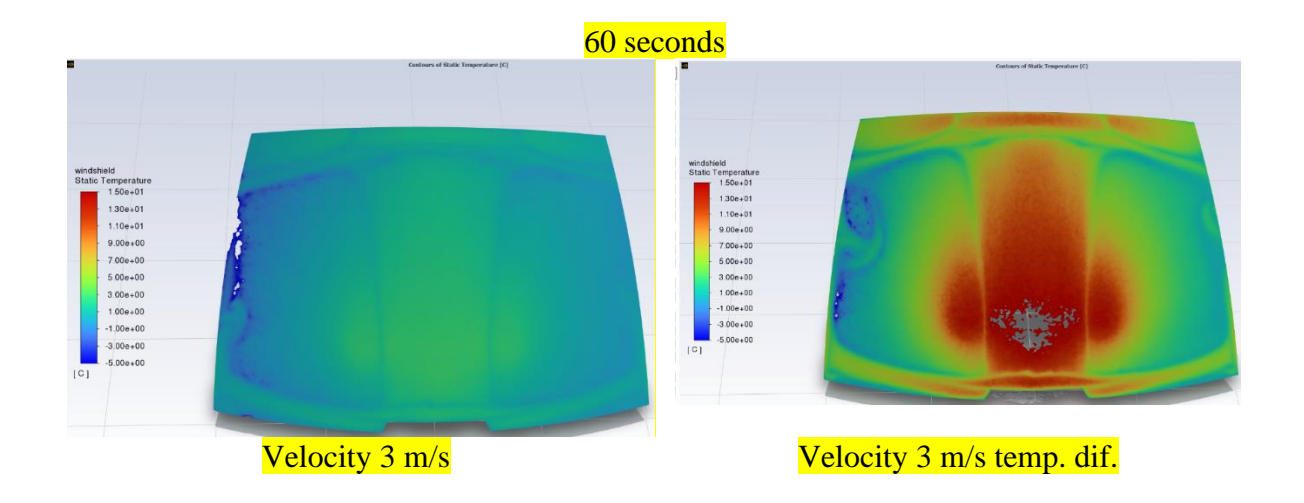
After 20 seconds of demisting grids being set into function, an increase in temperature air supply starts to show its influence on the windshield's temperature contour as can be seen in Fig. 24. This explains why increasing the air temperature of the supply air does not have that much influence on the condensation process. As the air temperature first heats the centre of the windshield and the condensation process mainly takes place at the outer regions of the windshield, there is a need to increase the time in order to allow to this heated air to reach these regions as well.

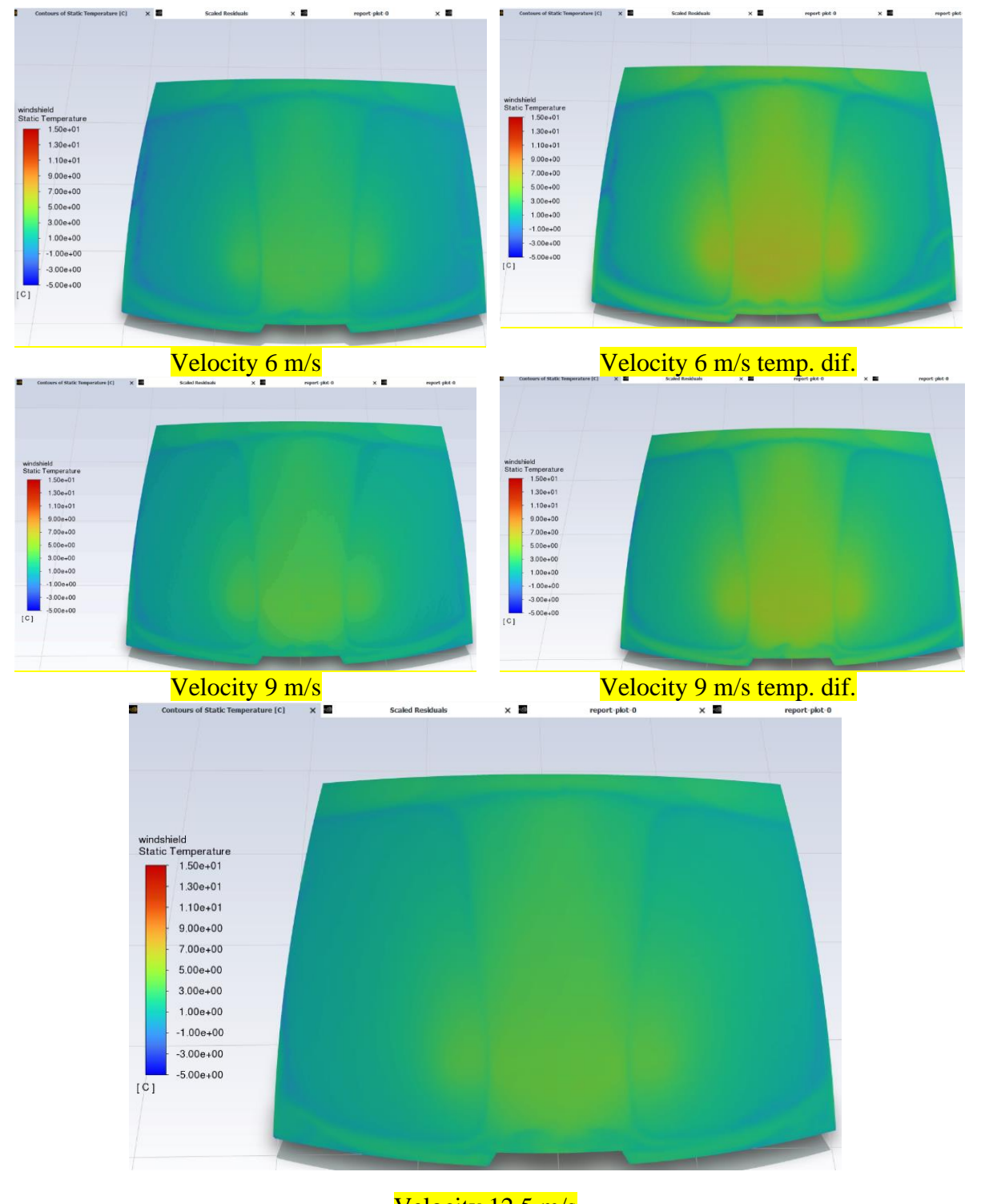




Velocity 12.5 m/s
Fig. 25 – Temperature contour on the windshield at 40 seconds

After 40 seconds of the heating system using the demisting grids into function, it can be seen that the temperature contour on the windshield as described in Fig. 25 starts to be more visible. The air supply temperature starts to heat the windshield for the air velocity of 3 m/s at increased temperature, leading to an air supply temperature of around 13 °C. The other air velocities maintain lower temperatures at the windshield level, temperatures that do not exceed 7 °C. The air velocity of 12.5 m/s shows a uniformity in temperature contour.





Velocity 12.5 m/s
Fig. 26 – Temperature contour on the windshield at 60 seconds

Fig. 26 showcases the temperatures at 60 seconds for all velocities and air temperatures. It can be highlighted that the influence of air supply temperature starts to make a difference for the air velocities of 6 m/s and 9 m/s. Also, for the air velocity of 12.5 m/s it can be seen that the temperature remains uniform with a tendency to raise a bit in the middle of the windshield, in the region where the air grids are placed. The outer part of the windshield presents a lower value of around 2 °C.

5. Conclusions

The purpose of this study was to evaluate the condensation phenomenon on the windshield of a vehicle. This was done by means of a numerical CFD determination based on a single-phase model. This numerical model was successfully used in previous studies when a comparison between the numerical and experimental results was produced. The present study took this model to the next level by imposing the source term for the water vapours condensation on the face of the cells that were found at the interface between the fluid region and the windshield solid region. This aspect was intended in order to simulate as closer to reality as possible the condensation phenomenon on a solid surface. Several scenarios were assessed in order to delimitate the best option with regards to the condensation phenomenon taking place on the windshield of the vehicle and the energy consumption that is involved in this process. Therefore, the maximum air velocity was set to 12.5 m/s and based on this value, the thermal power of the heating system was determined. The temperature of the supply air was varied in time based on the values obtained by experimental approaches in literature. Six different scenarios were assessed for air velocities of 3 m/s, 6 m/s and 9 m/s for air supply temperature similar to the one imposed at 12.5 m/s and air temperatures differences based on the thermal power of the system.

The results showed that by increasing the air flow the condensation phenomenon drops significantly. Moreover, the air velocity of 12.5 m/s represents the best solution in decreasing the condensation phenomenon and reducing the humidity levels. The air velocity of 3 m/s results in the largest mass flow rate of water vapours condensation.

The comparison between the 12.5 m/s and the other three air supply velocities by increasing the air supply temperature at the corresponding values based on the thermal power of the system showed that the air flow corresponding to 12.5 m/s air velocity still maintains the lowest amounts of condensation even though the temperature of the supply air for 3 m/s velocity reaches almost 15 °C after 25 seconds (this is still not enough to greatly reduce the condensation phenomenon). As it was lately analysed, the windshield presents a higher temperature for the region next to the air grids, whist the condensation phenomenon generally is taking place at the outskirts of the region. Therefore, there is a need to increase the temperature on the entire windshield in order to reduce the condensation process. However, after 60 seconds of demisting system usage, the mass flow rate of water vapours condensation drops significantly for the air velocities of 12.5 m/s, 9 m/s and 6 m/s, whilst for an air velocity of the supply air of 3 m/s the condensation phenomenon still presents significant values. A raise of 250 % in the mass flow water vapours condensation for an air velocity of 3 m/s and air supply temperature increased, takes place in comparison with the air velocity of 12.5 m/s.

Changing the air temperature of the supply air is not sufficient to produce significant changes in the mass flow rate of water vapour condensation for the air velocities of 6 m/s and 9 m/s. Furthermore, a reduction in air flow leads to an energy consumption decrease by 0.29 kWh for the air velocity of 6 m/s and with the 0.19 kWh for the air supply velocity of 9 m/s.

For the air velocity of 3 m/s, corresponding an air flow of 0.04 m³/s, differences in air supply temperatures leads to an increase of thermal energy input of 0.6 kWh further results in

a decrease in mass flow rate of water vapours condensation of 0.186 g/s, meaning a reduction of 93% of the mass flow rate of water vapours condensation.

Also, the results did not show significant differences in the mass flow rate of water vapours condensation contours between the air temperatures of the supply air for the same air velocity, within the first seconds of the demisting grids utilisation, However, the differences start to gain terrain after around 20 seconds.

After 100 seconds the demisting system clears the windshield area from any water vapours condensation leading to a visible windshield at the air velocity of the supply air of 12.5 m/s. However, the air velocity of 9 m/s and 6 m/s regardless of the air temperature of the supply air still have some areas that need to continue de demisting process in order to provide a clear view.

It was discovered that at the beginning of the condensation process when it results in significant condensation quantities as for the air velocity of 3 m/s, a drop in the temperature on the windshield takes place. Although, the condensation phenomenon produces a heat release, the heat release is further leading to an increase in heat transfer phenomenon between the indoors and the outdoor environment. This phenomenon is also supported by the literature [25].

After 40 seconds, the air supply temperature starts to heat the windshield for the air velocity of 3 m/s and the thermal power modified accordingly, at around 20 °C. The other air velocities do not exceed the air temperature supply of 7 °C. In general, the air velocity of 12.5 m/s shows a uniformity in temperature contour.

6. Perspectives

The numerical study proposes another chapter where an evaluation of the condensation phenomenon on the windshield together with a heating source implementation. This new part includes another series of cases where the boundary conditions will be changed in order to obtain the best scenario between energy consumption and maintenance of the optimum visibility of the windshield while driving. Several electrical powers will be inserted on the windshield together with a variation of the water vapours mass sources in order to delimit the best ventilation rates while driving sessions.

References

- [1] Hannan M A, Azidin F A, and Mohamed A, Hybrid electric vehicles and their challenges: A review, *Renewable and Sustainable Energy Reviews*, **29**, pp. 135-150, 2014.
- [2] (2022, 25.08.2022). Primary and final energy consumption in Europe.
- [3] (February 2022, 25.08.2022). Energy statistics an overview.
- [4] Ibrahim A and Jiang F, The electric vehicle energy management: An overview of the energy system and related modeling and simulation, *Renewable and Sustainable Energy Reviews*, **144**, 2021.
- [5] (1 Jun 2022, 25.08.2022). Energy crisis: opportunity or threat for EU's energy transition?
- [6] Nurdiawati A and Agrawal T K, Creating a circular EV battery value chain: End-of-life strategies and future perspective, *Resources, Conservation and Recycling*, **185**, 2022.
- [7] Yanyan Tang Q Z, Hailong Li, Yaoming Li, Boyu Liu, Economic analysis on repurposed EV batteries in a distributed PV system under sharing business models, *Energy Procedia*, **158** pp. 4304–4310, 2019.
- [8] Gis M, Wiśniowski P, and Bednarski M, Efficiency of electric vehicle interior heating systems at low ambient temperatures, *Open Engineering*, **11**, no. 1, pp. 499-507, 2021.
- [9] Haram M H S M, Lee J W, Ramasamy G, Ngu E E, Thiagarajah S P, and Lee Y H, Feasibility of utilising second life EV batteries: Applications, lifespan, economics, environmental impact, assessment, and challenges, *Alexandria Engineering Journal*, **60**, no. 5, pp. 4517-4536, 2021.
- [10] Qi Z, Advances on air conditioning and heat pump system in electric vehicles A review, *Renewable and Sustainable Energy Reviews,* **38**, pp. 754-764, 2014.
- [11] S. M. Aceves J R S, A Desiccant Dehumidifier for Electric Vehicle Heating, *Journal of Energy Resources Technology*, 1998.
- [12] Zhang Z, Wang J, Feng X, Chang L, Chen Y, and Wang X, The solutions to electric vehicle air conditioning systems: A review, *Renewable and Sustainable Energy Reviews*, **91**, pp. 443-463, 2018.
- [13] Ayartürk H, Doruk E, Durgun İ, and Ekbiç K, New Heating System Development Working with Waste Heat for Electric Vehicles, *Transportation Research Procedia*, **14**, pp. 1080-1086, 2016.
- [14] Commission Regulation (EU) No. 672/2010 concerning type-approval requirements for windscreen defrosting and demisting systems of certain motor vehicles and implementing Regulation (EC) No 661/2009 of the European Parliament and of the Council concerning type-approval requirements for the general safety of motor vehicles, their trailers and systems, components and separate technical units intended therefor, 2010.
- [15] Peng Q and Du Q, Progress in Heat Pump Air Conditioning Systems for Electric Vehicles—A Review, *Energies*, **9**, no. 4, 2016.
- [16] Bellocchi S, Leo Guizzi G, Manno M, Salvatori M, and Zaccagnini A, Reversible heat pump HVAC system with regenerative heat exchanger for electric vehicles: Analysis of its impact on driving range, *Applied Thermal Engineering*, **129**, pp. 290-305, 2018.
- [17] Uwe Kohle W P, Robert Apfelbeck, Bioethanol Heater for the Passenger Compartments of Electric Cars, *Development Thermal Management*, **114**, 2012.
- [18] Ahn J H, Kang H, Lee H S, and Kim Y, Performance characteristics of a dual-evaporator heat pump system for effective dehumidifying and heating of a cabin in electric vehicles, *Applied Energy*, **146**, pp. 29-37, 2015.
- [19] Chang T-B, Sheu J-J, and Huang J-W, High-Efficiency HVAC System with Defog/Dehumidification Function for Electric Vehicles, *Energies*, **14**, no. 1, 2020.
- [20] San-Juan M, Martín Ó, Mirones B J, and De Tiedra P, Assessment of efficiency of windscreen demisting systems in electrical vehicles by using IR thermography, *Applied Thermal Engineering*, **104**, pp. 479-485, 2016.

- [21] Karim J. Nasr B A N, Temperature Measurement of a Vehicle's Windshield Using Liquid Crystals, SAE 2002 World Congress Detroit, Michigan, March 4-7, 2002, 2002.
- [22] Zhang G, Zou H, Qin F, Xue Q, and Tian C, Investigation on an improved heat pump AC system with the view of return air utilization and anti-fogging for electric vehicles, *Applied Thermal Engineering*, **115**, pp. 726-735, 2017.
- [23] LEE D, Experimental study on the heat pump system using R134a, *International Journal of Automotive Technology*, **Vol. 16**, p. pp. 923–928 2015.
- [24] Bejan A, Convection Heat Transfer. John Wiley & Sons, Inc., Hoboken, New Jersey, 2013.
- [25] Duan Q, Hinkle L, Wang J, Zhang E, and Memari A, Condensation effects on energy performance of building window systems, *Energy Reports*, **7**, pp. 7345-7357, 2021.
- [26] Nguyen C-K, Teodosiu C, Kuznik F, David D, Teodosiu R, and Rusaouën G, A full-scale experimental study concerning the moisture condensation on building glazing surface, *Building and Environment*, **156**, pp. 215-224, 2019.
- [27] Liu J, Aizawa H, and Yoshino H, CFD prediction of surface condensation on walls and its experimental validation, *Building and Environment*, **39**, no. 8, pp. 905-911, 2004.
- [28] You S, Li W, Ye T, Hu F, and Zheng W, Study on moisture condensation on the interior surface of buildings in high humidity climate, *Building and Environment*, **125**, pp. 39-48, 2017.
- [29] ANSYS Fluent Theory Guide 2015.
- [30] Teodosiu R, Integrated moisture (including condensation) Energy–airflow model within enclosures. Experimental validation, *Building and Environment*, **61**, pp. 197-209, 2013.
- [31] Ilie V, Studiul Fenomenelor de Transfer de Căldură și Masă in Încăperi Climatizate, 2017.
- [32] Han J-W, Zhu W-Y, and Ji Z-T, Comparison of veracity and application of different CFD turbulence models for refrigerated transport, *Artificial Intelligence in Agriculture*, **3**, pp. 11-17, 2019.
- [33] Li X and Tu J, Evaluation of the eddy viscosity turbulence models for the simulation of convection—radiation coupled heat transfer in indoor environment, *Energy and Buildings*, **184**, pp. 8-18, 2019.
- [34] Menchaca-Brandan M A, Dominguez Espinosa F A, and Glicksman L R, The influence of radiation heat transfer on the prediction of air flows in rooms under natural ventilation, *Energy and Buildings*, **138**, pp. 530-538, 2017.
- [35] Li X, Yan Y, and Tu J, Evaluation of models and methods to simulate thermal radiation in indoor spaces, *Building and Environment*, **144**, pp. 259-267, 2018.
- [36] Hohota R, "Modelisation de l'humidite dans un code CFD (basses vitesses en grand cavite). Compairasonavec l'experimental.," Ph.D Thesis, Institut National des Sciences Appliquees de Lyon

2003.

- [37] ANSYS Fluent UDF Manual, Release 15.0 ed.
- [38] Kambiz Jahani S B, Utilizing CFD Approach for Preeminent Assessment of Defroster Air Flow Distribution and Predicting Windscreen Deicing Behavior, presented at the SAE Technical Paper Series, 2014.
- [39] Sadananda T, "Improving the Accuracy of CFD Method for Windscreen Deicing," Chalmers University of Technology Goteborg, Sweden Disertation Thesis, 2016.
- [40] Fayazbakhsh M A and Bahrami M, Comprehensive Modeling of Vehicle Air Conditioning Loads Using Heat Balance Method, presented at the SAE Technical Paper Series, 2013.
- [41] Mao Y, Wang J, and Li J, Experimental and numerical study of air flow and temperature variations in an electric vehicle cabin during cooling and heating, *Applied Thermal Engineering*, **137**, pp. 356-367, 2018.
- [42] Han U, Kang H, Song J, Oh J, and Lee H, Development of dynamic battery thermal model integrated with driving cycles for EV applications, *Energy Conversion and Management*, **250**, 2021.

[43]	HENS H, "IEA Annex 14: Condensation and Energy," Department of Civil Engineering, Laboratory of Building Physics, Belgium, JOURNAL OF THERMAL INSULATION 1992.